Published in final edited form as:

Traffic. 2024 January ; 25(1): e12927. doi:10.1111/tra.12927.

Rescue of secretion of rare-disease associated misfolded mutant glycoproteins in *UGGT1* knock-out mammalian cells

Gabor Tax[1], **Kevin P. Guay**[2], **Ludovica Pantalone**[3], **Martina Ceci**[3], **Tatiana Soldà**[4], **Charlie J. Hitchman**[1], **Johan C. Hill**[5], **Snežana Vasiljević**[5], **Andrea Lia**[1,6], **Carlos P. Modenutti**[7], **Kees R. Straatman**[8], **Angelo Santino**[6], **Maurizio Molinari**[5,9], **Nicole Zitzmann**[5], **Daniel N. Hebert**[2], **Pietro Roversi**[#,1,10], **Marco Trerotola**[#,3]

[1]Leicester Institute of Chemical and Structural Biology and Department of Molecular and Cell Biology, University of Leicester, Henry Wellcome Building, Lancaster Road, Leicester LE1 7HR, England, United Kingdom.

[2]Department of Biochemistry and Molecular Biology, and Program in Molecular and Cellular Biology, University of Massachusetts, Amherst, United States.

[3]Department of Medical, Oral and Biotechnological Sciences, "G. d'Annunzio" University of Chieti-Pescara, Italy; Laboratory of Cancer Pathology, Center for Advanced Studies and Technology (CAST), "G. d'Annunzio" University of Chieti-Pescara, Italy.

[4]Institute for Research in Biomedicine, Faculty of Biomedical Sciences, UniversitàdellaSvizzeraItaliana (USI), Bellinzona, Switzerland.

[5]Institute of Glycobiology, Department of Biochemistry, South Parks Road, Oxford OX1 3RQ, United Kingdom.

[6]Institute of Sciences of Food Production, ISPA-CNR Unit of Lecce, via Monteroni, I-73100 Lecce, Italy.

[7]Departamento de QuímicaBiológica, Facultad de Ciencias Exactas y Naturales, Universidad de Buenos Aires (FCEyN-UBA) e Instituto de QuímicaBiológica de la Facultad de Ciencias Exactas y Naturales (IQUIBICEN) CONICET, Pabellón 2 de Ciudad Universitaria, Ciudad de Buenos Aires C1428EHA, Argentina

[8]Core Biotechnology Services, University of Leicester, University Road, Leicester LE1 7RH, England, United Kingdom.

[9]School of Life Sciences, École Polytechnique Fédérale de Lausanne, Lausanne, Switzerland.

Correspondence: Marco Trerotola: marco.trerotola@unich.it; Pietro Roversi: pietro.roversi@cnr.it.
[#]:these authors contributed equally

Author contributions. P.R. and M.T. conceived the study. C.P.M. and P.R. carried out the *in silico* work. D.N.H., K.P.G., M.M., T.S, J.C.H., L.P., S.V. and N.Z. generated the KO cells. G.T. and M.T. carried out cloning of the vectors for transfections and established the transfection and fluorescence microscopy protocols. G.T. and K.R.S. carried out the fluorescence microscopy measurements on HEK293T cells. M.T., L.P. and M.C. carried out the fluorescence microscopy measurements on Vero E6 and KM12SM cells, the flow cytometry experiments, and the functional assays. G.T., K.R.S. and M.T. analysed the fluorescence microscopy data. G.T., A.L., A.S., P.R. and C.J.H. carried out the biochemical characterisation of the WT and mutant glycoproteins. K.P.G. and D.N.H. assayed reglucosylation*in cellula*. All authors were involved in the data analysis and the writing of the manuscript.

Conflicts of Interest: Nil.

Ethics statement: An ethical statement is not required for this research.

[10]Institute of AgriculturalBiology and Biotecnology, IBBA-CNR Unit of Milano, via Bassini 15, I-20133 Milano, Italy.

Abstract

Endoplasmic reticulum (ER) retention of misfolded glycoproteins is mediated by the ER-localised eukaryotic glycoprotein secretion checkpoint, UDP-glucose glycoprotein glucosyl-transferase (UGGT). The enzyme recognises a misfolded glycoprotein and flags it for ER retention by re-glucosylating one of its *N*-linked glycans. In the background of a congenital mutation in a secreted glycoprotein gene, UGGT-mediated ER retention can cause rare disease, even if the mutant glycoprotein retains activity ("responsive mutant"). Using confocal laser scanning microscopy, we investigated here the subcellular localisation of the human Trop-2-Q118E, E227K and L186P mutants, which cause gelatinous drop-like corneal dystrophy (GDLD). Compared with the wild type Trop-2, which is correctly localised at the plasma membrane, these Trop-2 mutants are retained in the ER. We studied fluorescent chimeras of the Trop-2 Q118E, E227K and L186P mutants in mammalian cells harbouring CRISPR/Cas9-mediated inhibition of the *UGGT1* and/or *UGGT2* genes. The membrane localisation of the Trop-2 Q118E, E227K and L186P mutants was successfully rescued in $UGGT1^{-/-}$cells. UGGT1 also efficiently reglucosylated Trop-2-Q118E-EYFP *in cellula*. The study supports the hypothesis that UGGT1 modulation would constitute a novel therapeutic strategy for the treatment of pathological conditions associated to misfolded membrane glycoproteins (whenever the mutation impairs but does not abrogate function), and it encourages the testing of modulators of ER glycoprotein folding quality control as broad-spectrum rescue-of-secretion drugs in rare diseases caused by responsive secreted glycoprotein mutants.

Graphical Abstract

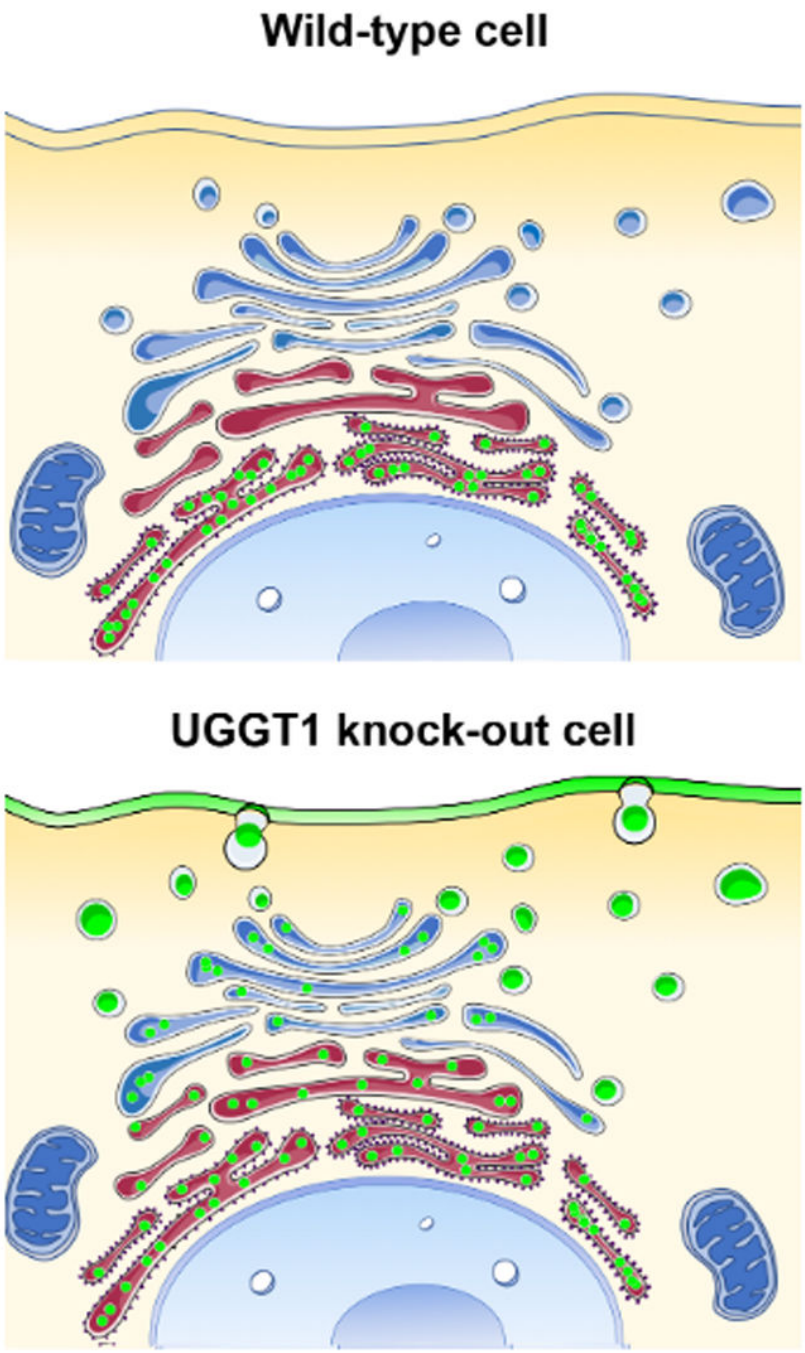

"The figure depicts the transformative impact of UGGT1 gene deletion in mammalian cells on the intracellular fate of fluorescent chimeras representing human Trop-2 Q118E, E227K, and L186P glycoprotein mutants, implicated in gelatinous drop-like corneal dystrophy. In wild type cells (*UGGT1*$^{+/+}$), the mutants are ensnared within the endoplasmic reticulum (ER), symbolized by the trapped green protein. Conversely, in UGGT1 knockout cells (*UGGT1*$^{-/-}$), the green protein successfully navigates to the cell membrane, illustrating the rescue of secretion. Notably, the Trop-2-Q118E glycoprotein, a disease mutant, undergoes efficient glucosylation by UGGT1 in human cells, establishing its classification as a genuine cellular UGGT1 substrate."

Keywords

responsive mutant; glycoprotein secretion; UGGT; UGGT1; UGGT2; GDLD; Trop-2; *TACSTD2*

Introduction

The endoplasmic reticulum (ER) glycoprotein folding quality control (ERQC) and ER associated degradation (ERAD) protein machineries survey glycoprotein folding in the early secretory pathway. Both systems rely on checkpoint enzymes for detection of misfolded glycoproteins. A glycoprotein that has not yet attained its native fold in the ER is recognised as misfolded by the ERQC checkpoint enzyme, UDP-glucose glycoprotein glucosyltransferase (UGGT). UGGT flags a misfolded glycoprotein for ER retention by re-glucosylating one of its glycans, thus enabling ER lectin-associated chaperones (calnexin and calreticulin) and foldases to aid its folding [1]. After prolonged cycles of UGGT-mediated ER retention, a terminally misfolded glycoprotein in the ER is eventually recognised by the checkpoint of ERAD (a complex between an ER degradation-enhancing mannosidase, EDEM, and a protein disulphide isomerase, PDI), which de-mannosylates it, and dispatches it to retro-translocation and degradation in the cytoplasm [2]. The ERQC/ERAD pathways provide means of coping with ER stress, ensure steady state glyco-proteostasis, prevent premature secretion of slowly folding glycoproteins and dispose of terminally misfolded ones, thus conferring evolutionary advantages to healthy eukaryotic cells [3].

In the background of a secreted glycoprotein gene mutation that does not completely abrogate glycoprotein activity ("responsive mutant" [4]), the stringency of the ERQC/ERAD machineries can be detrimental: UGGT recognises the mutated glycoprotein and flags it for ER retention, and the ERAD checkpoint de-mannosylates it, leading to degradation of the mutant glycoprotein, and to the concomitant loss of its residual activity. A variety of devastating congenital rare diseases are indeed caused by overzealous ERQC/ERAD checkpoints preventing secretion of responsive mutant glycoproteins [5].

Replacement of the mutated gene with a wild type (WT) copy (gene therapy [6]) has the potential to help patients affected by congenital rare diseases. A second therapeutic strategy – whenever the patient's mutation alters a gene encoding an enzyme – is enzyme replacement therapy [7]. A third strategy to help the subset of patients carrying responsive mutations is the use of a pharmacological chaperone [4]. A fourth, so far unexplored avenue for the therapy of congenital rare diseases caused by responsive glycoprotein mutants would be molecules modulating the ERQC/ERAD checkpoint enzymes, which could act as rescue-of-secretion drugs [8,9]. Deletion of either the ERQC or ERAD misfolding checkpoints can indeed rescue secretion of glycoprotein responsive mutants in the cress *Arabidopsis thaliana*[10,11]; inhibition of human ERAD mannosidases also rescues the secretion of a ß-sarcoglycan missense mutant [12]. No published study to date has investigated modulation of UGGT activity as a means of rescuing secretion of a human rare disease-associated responsive mutant glycoprotein.

Two paralogues of UGGT exist within the ER (UGGT1 and UGGT2). Only a few physiological clients of UGGT1 had been described [10,13-18] and the first partly overlapping

subsets of UGGT1and UGGT2 client glycoproteins (the "UGGT-omes" [19]) have only recently been characterised in HEK293 cells [20]. It is therefore not surprising that the role of UGGT in deciding the secretory trajectory of misfolded glycoprotein mutants has been little studied in mammalian cells [9,14,21,22]. The mammalian UGGT1 isoform is essential during early embryogenesis and the homozygous *UGGT1*$^{-/-}$ genotype causes mouse embryonic lethality, although cells derived from those embryos are viable [15]. Heterozygous *UGGT1*$^{+/-}$ mice have been reported to express approximately half of the WT amount of UGGT1 and yet undergo normal development without any aberrant phenotype [23].

To date, there are no known UGGT selective inhibitors. UGGT is inhibited by its product UDP [24] and by squaryl derivatives of UDP [25]; by the non-hydrolysable UDP-glucose (UDP-Glc) cofactor analogue UDP-2-deoxy-2-fluoro-D-glucose (U2F); and by synthetic analogues of the *N*-linked $Man_9GlcNAc_2$ glycan substrate [26,27]. Obviously, none of these molecules are UGGT-specific. Recently, a fragment-based lead discovery effort [28] yielded a UGGT1 and UGGT2 inhibitor, which is being chemically modified to increase its affinity and selectivity[29]. At the moment, *UGGT* gene knockout (KO), as a limiting case of inhibition, represents the only amenable strategy to probe the role of the enzyme in ER retention of glycoproteins.

In this manuscript, we describe rescue-of-secretion experiments of congenital rare disease associated mutants of the membrane glycoprotein Trop-2 (*aka* epithelial glycoprotein-1, gastrointestinal antigen 733-1, membrane component surface marker-1, or tumour-associated calcium signal transducer-2). This glycoprotein plays various roles in physiological and pathological contexts, among which cell-cell and cell-substrate interactions, cancer growth and metastasis [30-33]. Human Trop-2 (from now on indicated as Trop-2) is encoded by the *TACSTD2* gene, whose nonsense and missense mutations have been reported to cause gelatinous drop-like corneal dystrophy (GDLD, OMIM #204870) [34,35], a congenital rare disease that was first described in 1914 in a Japanese patient [36,37]. Since then, most of the GDLD cases were reported in individuals carrying mutations in the *TACSTD2* gene, in Japanese, Indian, Sudanese, white and Chinese populations [38]. The worldwide prevalence of the disease is unknown; its frequency in Japan is estimated to be about 1/30,000, with about 4000 people affected by this disorder across the country. As is the case for the majority of congenital rare diseases, no cure is currently available for GDLD.

Patients with GDLD show a facilitated tear fluid permeation into their corneal tissue, and subepithelial amyloid deposition of lactoferrin; with ageing, the amyloid depositions typically enlarge, increase in number and coalesce with each other, leading to severe bilateral vision loss [39]. The *Tacstd2*$^{-/-}$ mouse was recently developed and found to show a phenotype similar to that of human GDLD, although the corneal opacities developed in these aged mice were mild only [40]. Several missense mutations of the *TACSTD2* gene have been reported to cause GDLD [41], but given that only the *Tacstd2*$^{-/-}$ mouse is available, alternative animal models are still required for fully investigating candidate responsive Trop-2 mutants *in vivo*.

Our experiments were conducted in WT and *UGGT1*$^{-/-}$, *UGGT2*$^{-/-}$ and *UGGT1/2*$^{-/-}$ HEK293T, Vero E6 and KM12SM mammalian cells. Fluorescent chimeras of enhanced yellow fluorescent protein (EYFP) C-terminally fused to WT or mutant Trop-2 were imaged by confocal laser scanning microscopy. For our *in cellula* study, we initially selected the GDLD-associated Trop-2-Q118E mutant [38] on the grounds that – upon modelling *in silico* the extracellular domain of Trop-2 and its missense mutants - the mutation seemed unlikely to impair function. In our experiments, we observe retention of Trop-2-Q118E-EYFP in WT and *UGGT2*$^{-/-}$ cells, and rescue of secretion and plasma membrane localisation of the same mutant in *UGGT1*$^{-/-}$ and *UGGT1/2*$^{-/-}$ cells. Pull-down experiments with recombinantly produced GST-tagged calreticulin (CRT) in human cell lysates using the KO background of dolichyl pyrophosphate $Man_9GlcNAc_2$ α−1,3-glucosyltransferase 6 (*ALG6*$^{-/-}$) [20] demonstrate that the Trop-2-Q118E-EYFP mutant is indeed glucosylated by UGGT1 *in cellula.* Two more Trop-2 mutants (E227K and L186P) were also retained in intracellular compartments of *UGGT1*$^{+/+}$ cells and were efficiently rescued to the secretory route towards the plasma membrane in *UGGT1*$^{-/-}$ cells.

SDS-PAGE and flow cytometry analysis of Trop-2-Q118E suggests that the majority of the secreted glycoprotein is aggregated via inter-molecular disulphides, making it unlikely that the mutant is responsive. Consistent with this, in functional Trop-2 assays, none of the Trop-2 mutants whose secretion is rescued by UGGT1 deletion can raise intracellular Ca^{2+} levels, which indicates that their folding defect largely impairs or abrogates function. Nevertheless, as it is likely that ERQC causes retention of many other responsive glycoprotein mutants involved in the onset and progression of congenital pathologies, our results encourage development and testing of modulators of ER glycoprotein folding as broad-spectrum rescue-of-secretion drugs in rare diseases associated with responsive glycoprotein mutants.

Results

Homology modelling the Trop-2-Q118E mutant glycoprotein suggests mildly impaired protein folding

Distinct GDLD-causing missense mutations of Trop-2 have been reported. For our rescue of secretion study, we initially set out to select the least fold-disrupting of the known GDLD-causing missense mutations of Trop-2. In order to evaluate the likely impact of each mutation, we started by building a homology model of the dimer of the mature portion of human Trop-2 (Uniprot P09758, TACD2_HUMAN). Besides the AlphaFoldMultimer model [42], a model was also built using Modeller [43]: the extracellular portion of the dimer (residues 27-268) was generated using as templates two distinct crystal structures of the cis-dimer of the same region of human Trop-2 (PDB IDs 7PEE [44] and 7E5N [45]); the transmembrane region (residues 278-298) was based on the NMR-derived model of the transmembrane portion of the rat p75 protein (PDB ID 4MZV, 30% sequence identity over 21 residues); the cytoplasmic domain of human Trop-2 (residues 299-323) was based on the NMR structure of the C-term of Trop-2 (PDB ID 2MAE).

We then examined the likely consequences of GDLD-associated missense mutations by mapping them onto the Trop-2 homology model. GDLD-associated mutations C108R and

C119S are likely to cause severe misfolding accompanied by severe loss of function, as both Cys residues are involved in a disulphide bond in the extracellular domain. GDLD-associated mutations Y184C, L186P and V194E are also very likely to cause severe misfolding, as they will alter the protein hydrophobic core constituted by F180, F190, I203, L205, I219, A222 and F226. This area of the protein is distal to the membrane and it is involved in the trans dimer-of-dimers that establishes cell-cell adhesions [45]. The charge-reversal mutation E227K sits close to the dimer interface, surrounded by three positively charged residues: K72, K231 and R228: this is likely to destabilise the monomer and/or cause loss of protein dimerisation. The L186P mutation affects a small surface pocket not too far from the membrane. The mutation Q118E appeared to be the best candidate for a putative responsive mutation: E is isosteric to Q, and the mutation appears to affect only a surface area of the protein immediately above the membrane (Figure S1).

Molecular dynamics of WT and Q118E Trop-2 extracellular dimer suggests that the Q118E mutation disrupts protein tertiary and quaternary structure

In order to estimate the impact of the Q118E mutation on the Trop-2 dimer structure, we performed 1 μs all-atom molecular dynamics (MD) simulations of the extracellular domain of the WT Trop-2 dimer and of the corresponding Q118E mutant. The global stability of the extracellular domain dimers in time can be followed by measuring the root mean square deviation ($rmsd_{C\alpha}$) of the protein backbone throughout the simulation, with the starting model taken as the reference. The Q118E mutant shows higher $rmsd_{C\alpha}$ values than the WT, indicating that the mutation affects the stability of the protein fold (Figure S2). In order to identify the regions most affected by the mutation, we measured the root mean square fluctuation ($rmsf_{C\alpha}$) during the simulation, again using the starting structure as a reference. Both mutant and WT proteins show high $rmsf_{C\alpha}$ values in N- and C-terminal regions. As expected, the thyroglobulin type-1 subdomain (TY, amino acids 70 to 145) is the region most affected by the Q118E mutation (Figure S3).In the WT structure, the sidechain of Q118 forms several hydrogen bonds that stabilise the domain (Figure S1). The mutation introduces an extra negative charge that results in electrostatic repulsion between D107 and E118; the backbone O of R115 is also interacting with the side chain of (Q)E118. The distributions of the values of the distance between the alpha carbons of residues D107 and Q(E)118 during the simulation give an estimate of the destabilisation local to the TY subdomain introduced by the mutation (Figure S4).

Secretion of the Trop-2-Q118E-EYFP mutant glycoprotein is impaired in WT HEK293T and Vero E6 cells

The Trop-2 Q118E mutant was initially chosen as a candidate to test rescue-of-secretion of a rare-disease associated missense glycoprotein mutant by modulation of UGGT.
In order to follow the subcellular localisation of the WT Trop-2 glycoprotein and its Trop-2-Q118E mutant, WT and *UGGT* KO mammalian cells (HEK293T, Vero E6) were transiently transfected with the Trop-2-pEYFP-N1 and Trop-2-Q118E-pEYFP-N1 plasmids, respectively encoding the EYFP C-terminal fusion of WT Trop-2 and its GDLD-associated Q118E mutant.

Localisation of the fluorescent fusion glycoproteins was visualised 48 hr post-transfection by confocal laser scanning microscopy imaging (Figures 1A, B). HEK293T imaging used live cells, while Vero E6 imaging was carried out on fixed cells. To assay membrane vs. ER localisation of Trop-2 fluorescent glycoprotein, we stained cell membranes with wheat germ agglutinin (WGA) Alexa Fluor 555 conjugate (orange, Figures 1C, D) and the ER with ER-Tracker Red (red, Figure S5). WGA membrane labelling is normally done on ice to avoid internalisation of the WGA signal by endocytosis. Indeed WGA can be used to image/measure endocytosis [46]. Due to the nature of the experiments to study the rescue of secretion, the experiments were performed at 37 °C, and some internalisation is visibile. Non transfected cells do not show any green/EYFP signal: this rules out autofluorescence (Figure S6). Control experiments in cells transfected with a plasmid encoding WT Trop-2-EYFP show the expected cell membrane localisation of the fusion glycoprotein, which traverses the secretory pathway and reaches the cell membrane in WT cells (Figures 1A, 1C and S5A, top row, white arrowheads). The Trop-2-Q118E-EYFP mutant glycoprotein is absent from the membrane and localises to the ER in WT human HEK293T and Vero E6 cells (Figures 1B, 1D and S5B, top row). The data suggest the Trop-2 Q118E mutant is also not secreted in GDLD patients carrying the mutation.

Secretion of the Trop-2-Q118E-EYFP mutant glycoprotein is rescued in *UGGT1* KO HEK293T and Vero E6 cells

To check if the observed ER retention of the Trop-2-Q118E-EYFP mutant glycoprotein is due to UGGT-mediated reglucosylation, single KO (*UGGT1*$^{-/-}$ and *UGGT2*$^{-/-}$) and double KO (*UGGT1/2*$^{-/-}$) HEK293T cells were transiently transfected alongside WT HEK293T control cells with Trop-2-pEYFP-N1 (green in Figures 1C and S5A) and Trop-2-Q118E-pEYFP-N1 plasmids (green in Figures 1D and S5B). The WGA fluorescence signal and the Trop-2-EYFP signal overlap in the plasma membrane (Figure 1C), suggesting that Trop-2-EYFP reaches the membrane in all cell lines. In the *UGGT1*$^{-/-}$ and *UGGT1/2*$^{-/-}$ merged images, the green Trop-2-Q118E-EYFP reaches the membrane and overlaps with the WGA signal (orange, Figure 1D, white arrowheads): secretion of the Trop-2-Q118E-EYFP mutant glycoprotein is rescued in absence of UGGT1. Partial rescue of secretion of Trop-2-Q118E-EYFP is also detectable in *UGGT2*$^{-/-}$ cells: the overlap of the green fluorescence with the Alexa Fluor 555 conjugate is less pronounced in *UGGT2*$^{-/-}$ cells than in the *UGGT1*$^{-/-}$ and *UGGT1/2*$^{-/-}$ cells (Figure 1D, white arrowheads).

Multichannel intensity plots [47] were used to measure the overlap between the different fluorophores in the cellular membrane (Figure 2). We were able to validate our initial observations. The Trop-2-EYFP protein signal co-localises with the WGA Alexa Fluor 555 marker in the plasma membrane in all cell lines (Figure 2, top panels). The Trop-2-Q118E-EYFP signal accumulates around the nucleus but not in the plasma membrane of WT HEK293T cells (Figure 2, bottom left panel). In absence of *UGGT* (*UGGT1*$^{-/-}$, *UGGT2*$^{-/-}$ and *UGGT1/2*$^{-/-}$), the mutant glycoprotein localises at the plasma membrane (Figure 2, all bottom panels but the leftmost one), although to a lesser extent than in WT Trop-2 transfected cells.

The plasma membrane was selected as region of interest (ROI) on the basis of WGA staining, and the green fluorescence intensity from WT Trop-2-EYFP and Trop-2-Q118E-EYFP was quantified in the ROI of WT HEK293T cells (Figure S7A). We then carried out the same analysis in UGGT KO cells as well. Fluorescence associated with Trop-2-EYFP was high in the plasma membrane in all HEK293T cell lines (Figure S7B). EYFP plasma membrane fluorescence in WT HEK293T cells transfected with Trop-2-Q118E-EYFP is around 25% of the signal observed for the same cells transfected with WT Trop-2-EYFP (Figure S7C). Plasma membrane fluorescence in *UGGT1*$^{-/-}$ and *UGGT1/2*$^{-/-}$ HEK293T cells transfected with Trop-2-Q118E-EYFP more than doubles compared to WT cells transfected with the same mutant (Figure S7C). *UGGT2*$^{-/-}$ cells show marginal Trop-2-Q118E-EYFP membrane signal improvement over WT cells (Figure S7C). These data quantitatively support the conclusion that secretion of Trop-2-Q118E is rescued upon UGGT1 KO.

The Trop-2-Q118E-EYFP lack of secretion phenotype is restored in HEK293T *UGGT1*$^{-/-}$ cells complemented with WT UGGT1 but not with inactive UGGT1

To check that the rescue of secretion observed for the Trop-2-Q118E-EYFP glycoprotein in the *UGGT1*$^{-/-}$ background is genuinely due to absence of UGGT1 catalytic activity in the KO cells, we performed UGGT1 complementation experiments. The previously generated WT and *UGGT1*$^{-/-}$ KO HEK293T cell lines were stably transfected with the *Hs*UGGT1-pCDNA3.1/Zeo(+) plasmid, encoding WT UGGT1, or with the *Hs*UGGT1-D1454A-pCDNA3.1/Zeo(+) plasmid, encoding an inactive mutant of UGGT1. The UGGT1 Asp1454 residue mutated in the latter plasmid is part of the conserved DQD motif in the catalytic domain [13,48] that likely bridges the substrate *N*-linked glycan and the UDP-glucose binding sites [13,29,49].

The localisation of the WT Trop-2-EYFP protein was not affected by the complementation (Figure 3A, and 3C top row panels). On the other hand, the Trop-2-Q118E-EYFP mutant glycoprotein was found to traverse the secretory pathway and reach the plasma membrane only in UGGT1 D1454A complemented *UGGT1*$^{-/-}$ cells (Figure 3B bottom row, and Figure 3C bottom row, third panel). The original lack of secretion phenotype and Trop-2-Q118E-EYFP glycoprotein retention was observed in all cells expressing WT UGGT1 (Figure 3B, first three rows and Figure 3C bottom row, first, second and fourth panels).

Intensity measurements of EYFP fluorescence in the plasma membrane confirmed the involvement of UGGT1 in the retention of Trop2-Q118E-EYFP in HEK293T cells (Figure S8). Trop-2-EYFP is evenly expressed in the plasma membrane in all cell lines (Figure S8A). In the *UGGT1*$^{-/-}$ cells complemented with WT UGGT1, we observe restoration of the original lack of secretion phenotype for Trop-2-Q118E-EYFP (Figure S8B). As expected, we still observe the partial rescue of secretion of the mutant glycoprotein in *UGGT1*$^{-/-}$ cells complemented with the inactive UGGT1 D1454A mutant (Figure S8B). These results confirm that UGGT1 likely causes ER retention of the Trop-2-Q118E-EYFP mutant glycoprotein.

The Trop-2-Q118E-EYFP mutant glycoprotein is efficiently glucosylated by UGGT1 *in cellula*

To confirm that ER retention of the mutant Trop-2-Q118E-EYFP glycoprotein is due to UGGT1, we assayed UGGT-mediated glucosylation of WT and mutant Trop-2-EYFP, transiently expressed into *ALG6*$^{-/-}$ HEK293T cells. During the synthesis of *N*-linked glycans, as dolichol-phosphate linked precursors, ALG6 appends the first glucose to the immature $Man_9GlcNAc_2$ *N*-linked glycan precursor, which is further built up by additional ALG proteins within the ER; the resulting $Glc_3Man_9GlcNAc_2$ glycan is finally transferred to nascent glycoproteins by an oligosaccharyltransferase (OST) (Figure 4A [50]). In WT cells, calnexin and CRT binding can occur either immediately after trimming of the OST-derived $Glc_3Man_9GlcNAc_2$ glycan to a $Glc_1Man_9GlcNAc_2$ form, by glucosidases I and II; or through reglucosylation of a $Man_9GlcNAc_2$ glycan by one of the UGGTs [1]. Thus, any detected $Glc_1Man_9GlcNAc_2$ glycans on glycoprotein clients in *ALG6*$^{-/-}$ cells must derive from UGGT glucosylation, and not from ER-glucosidase mediated partial *N*-linked glycan trimming of the OST-derived glycan (Figure 4B). The pool of UGGT-glucosylated glycoproteins was further enriched in our experiments in *ALG6*$^{-/-}$ cells by treating the cells with the glucosidase I and II inhibitor N-butyl-deoxynojirimycin (DNJ).

Single KO (*ALG6*$^{-/-}$) cells, as well as double KO (*ALG6/UGGT1*$^{-/-}$ and *ALG6/UGGT2*$^{-/-}$) and triple KO (*ALG6/UGGT1/2*$^{-/-}$) cells were transiently transfected with Trop-2-pEYFP-N1 or Trop-2-Q118E-pEYFP-N1 plasmids, to determine the levels of Trop-2 glucosylation and its specificity by either UGGT1 or UGGT2. Monoglucosylated Trop-2 was isolated from the single, double and triple KO cells using a recombinant GST-tagged CRT that specifically binds monoglucosylated glycoproteins. Any background or lectin-independent binding of monoglucosylated glycoproteins was measured and subtracted using a lectin-deficient variant of CRT, CRT(Y109A) [51]. The adjusted value was then divided by the amount of substrate within the whole cell lysate (WCL) in order to quantify the percent glucosylation (Figure 4C and E [20]).

Both the WT and Q118E mutant Trop-2 are glucosylated by UGGT (Figure 4C, lane 2) and are substrates specifically of UGGT1 (Figure 4C, lane 8). Minimal glucosylation is attributed to UGGT2 (Figure 4C, lane 5). As expected, no glucosylation is observed in the triple KO (Figure 4C, lane 12). Of note, no Trop-2 is observed in any CRT(Y109A) control pulldowns (Figure 4C, lanes 3, 6, 9, 12). The double band observed in the WCL lanes is likely due to the physiological cleavage of Trop-2 [31].

Glycosidase assay in WT, *ALG6*$^{-/-}$ and UGGT*1*$^{-/-}$ cells verified the identity of the multiple bands observed in Figure 4: these include a complex glycosylated mutant band in the UGGT*1*$^{-/-}$ cells ("Trop2^{Comp}", Figure S9). While Trop-2-EYFP and Trop-2-Q118E-EYFP overexpressed in *ALG6*$^{-/-}$ HEK293T cells produce multiple species (Figure 4C, lanes 1, 4, 7, and 10), a single major band is detected for both constructs when expressed in WT cells (Figure S9, lanes 1 and 4). Hypoglycosylation of some glycoproteins has been reported in *ALG6*$^{-/-}$ HEK293T cells [20]. Hypoglycosylation of the Trop-2 constructs is apparent, as treatment with PNGaseF collapses the bands into a single deglycosylated species ("Trop2^{NG}", Figure S9, lanes 8 and 11). It is also possible that the fastest migrating band observed upon expression in the *ALG6*$^{-/-}$ cells corresponds to untranslocated and

unglycosylated protein as it migrates similarly to the glycosidase treated species (Figure S9, lanes 7-12). Additionally, when expressed in WT cells, the migration of Trop-2-EYFP and Trop-2-Q118E-EYFP differs (Figure S9, lanes 8 and 11). This is due to the presence of complex glycans on Trop-2-EYFP that egresses through the Golgi. Trop-2-Q118E-EYFP is ER retained and contains only high mannose glycans, which are lower in molecular mass ("Trop2^{HM}", Figure S9, lane 4). This is confirmed by EndoH treatment, as there is a significant shift in the migration of Trop-2-Q118E, while the majority of the WT Trop-2 is resistant to EndoH digestion (Figure S9, lanes 3 and 6). However, EndoH resistant complex sugars are observed on Trop-2-Q118E-EYFP when UGGT1 is absent, indicative of Golgi trafficking and furthering supporting a role of UGGT1 in mediating the ER retention of the mutant protein (Figure S9, lane 18).

The Q118E substitution significantly increases the recognition and glucosylation by UGGT1 in both *ALG6*$^{-/-}$ and *ALG6/UGGT2*$^{-/-}$ cell lines (Figure 4C, lanes 2, 8 and Figure 4E). Levels of glucosylation increase from ~10% to ~60%, for the WT and Q118E mutant respectively, in both the *ALG6*$^{-/-}$ and *ALG6/UGGT2*$^{-/-}$ cells. Minimal glucosylation is observed within the *ALG6/UGGT1*$^{-/-}$ cell line with no significant difference to WT being measured. Taken together, these results demonstrate that both the WT and mutant Trop-2 are efficiently glucosylated within the ER and the Q118E mutation significantly increases the amount of glucosylation by UGGT1. This suggests that the likely mechanism for the failure of the mutant to traffic to the cell surface is through increased reglucosylation by UGGT1, and subsequent lectin chaperone binding, leading to ER retention of the mutant.

The Q118E mutation results in increased inter-molecularly SS-bonded misfolded Trop-2 multimers

To acquire insight on the nature of the misfolding recognised by UGGT1 in the Trop-2-Q118E-EYFP mutant, we analysed (by Western blotting with an anti-EYFP antibody) membrane fractions from cells transiently transfected with the Trop-2 WT and Q118E mutant glycoproteins. Membrane fractions were isolated with CelLytic MEM Protein Extraction Kit ™ (Figure 5). Inter-molecularly SS-bonded Trop-2 multimers are detected in small amounts in all membrane samples under non-reducing conditions. The amounts of these inter-molecularly SS-bonded multimers increase when the cells express the Trop-2-Q118E mutant (Figure 5, left-hand side).

Multiparametric flow cytometry confirms that secretion of misfolded Trop-2-Q118E mutant is rescued in *UGGT1*$^{-/-}$cells

Biochemical analysis suggested that the majority of the secreted Trop-2-Q118E mutant is aggregated via inter-molecular disulphides. We further probed the structural integrity of the rescued Trop-2 mutants by multiparametric flow cytometry on *UGGT1*$^{-/-}$ Vero E6 cells expressing WT or Q118E Trop-2-EYFP fusion glycoproteins (Figure 6). Specifically, we stained these cells with two different types of far-red (APC) labelled antibodies: a conformation-insensitive goat polyclonal antibody (pAb, AF650 from R&D) and the T16 mouse monoclonal antibody (mAb), which only binds the native/correctly folded Trop-2 [52]. Neither antibody bound mock-transfected cells expressing EYFP (Figure 6A). Hence, we gated out EYFP^{+} cells and compared the mean fluorescence intensities (MFIs) of the

cells stained with mAb and pAb in order to discriminate between misfolded (ratio < 1) and correctly folded (ratio ≥1) Trop-2 (Figure 6B). Staining of *UGGT1*$^{+/+}$ Vero cells expressing WT or Q118E Trop-2-EYFP showed that the WT molecule was easily recognised by both Abs (Figure 6C, top panel), while neither the mAb nor the pAb was able to bind the Q118E mutant (Figure 6C, bottom panel). On the other hand, staining of *UGGT1*$^{-/-}$ Vero cells expressing WT or Q118E Trop-2-EYFP showed that the WT molecule was bound by both Abs (mAb/pAb MFI ratio = 1.63), while the Q118E mutant was predominantly bound by the pAb (mAb/pAb MFI ratio = 0.21) (Figure 6D). This analysis confirms that the secretion of the Trop-2-Q118E mutant is rescued upon KO of *UGGT1*, although the mutant is to some extent structurally compromised.

Rescued secretion of the misfolded Trop-2 mutants is not accompanied by restoration of Trop-2 function

Trop-2 is a key driver of human cancer cell growth and stimulates Ca^{2+}signaling[32]. As flow cytometry suggests that the structural integrity of the Trop-2-Q118E mutant might be compromised (Figure 6), we hypothesised that the biological function of the molecule might also be impaired. We performed *in vitro* proliferation assays of human colorectal cancer KM12SM cells overexpressing WT or Q118E Trop-2-EYFP fusion glycoproteins. As shown in figure S10, the Q118E Trop-2 mutant is unable to stimulate cell proliferation as the WT molecule does, neither in presence nor in absence of UGGT1.

To further consolidate our approach of rescue-of-secretion through modulation of UGGT1, we investigated two additional Trop-2 variants associated with GDLD, specifically the Trop-2-E227K and the Trop-2-L186P mutants. We modelled these two mutations *in silico* in the context of a Trop-2 dimer (Figure S11). E227 is visible in white spheres in Figure S11A. In the WT molecule, this residue forms a salt bridge with K231 (black spheres in Figure S11A) inside the core cavity at the centre of the dimer: thus, the E227K mutation likely introduces an excess of up to two non-neutralized positive charges to the cavity at the centre of the dimer. L186 is visible in white spheres in Figure S11B. The mutation affects a small surface pocket not too far from the membrane. It likely weakens the packing of Trop-2 loop 183-190 (between the α helix 168-182 and the β strand 191-197) against the beginning of the α helix 219-231.

UGGT1$^{+/+}$ and *UGGT1*$^{-/-}$ Vero cells were transfected with two different fluorescently labelled sets of Trop-2 molecules: WT Trop-2-EYFP (in order to track the localization of the non-mutated protein in the cell), and WT or mutant Trop-2-mCherry (in order to track Trop-2 mutants secretion to the cell membrane). Q118E, E227K and L186P Trop-2 mutants were retained in intracellular compartments of *UGGT1*$^{+/+}$ cells (Figure 7, left-hand side), and were efficiently rescued to the secretory route towards the plasma membrane in *UGGT1*$^{-/-}$ cells (Figure 7, right-hand side).

We then performed double transfections of KM12SM cells with Trop-2-EYFP (WT or Q118E or E227K or L186P) in presence of a red fluorescent genetically encoded calcium indicator (CMV-R-GECO1.2) [53] in order to assess the Ca^{2+} transducing activity of Trop-2 upon specific antibody crosslinking. All three mutants failed to transduce a Ca^{2+} signal

(Figure S12) suggesting that these GDLD-associated point mutations heavily compromise the biological activity of Trop-2.

Discussion

In the background of a congenital mutation in a gene encoding a secreted glycoprotein, the ER glycoprotein misfolding checkpoint enzymes (UGGTs and EDEMs) are likely responsible for prolonged ER retention and eventual degradation of the mutant glycoprotein [54]. This in turn gives rise to loss-of-function congenital rare disease. Thus, for a wide range of slightly misfolded but still functional glycoproteins ("responsive mutants" [4]), the fidelity of ERQC/ERAD paradoxically exacerbates the severity of disease [5,55,56]. Evidence of disease-associated lack of secretion exists for several rare disease associated glycoprotein mutants [57-60]. For patients carrying glycoprotein mutants that fail to reach the intended cellular or extracellular destination, enzyme replacement [7] is a viable option; if the mutant retains measurable residual activity, pharmacological chaperone therapy [61] is also possible.

For the subset of congenital rare disease patients carrying a responsive mutation, modulation of the ER glycoprotein misfolding checkpoint enzymes (UGGT/EDEM) is an alternative, yet-to-be-explored strategy to restore misfolded active glycoprotein secretion and alleviate the disease symptoms [8,9,56]. Unfortunately, databases of rare disease associated congenital missense mutations do not routinely report residual activity information [62]. Thus, the scope of rescue-of-secretion therapy - in terms of overall number of patients carrying responsive mutations across the full spectrum of congenital rare disease - is difficult to assess. Of course, for all glycoprotein clients that are either slow to fold and/or carry toxicity when misfolded, modulation of UGGT/EDEM of course carries an intrinsic risk of premature and unwanted secretion, a scenario we dubbed the "ER Pandora's box" [19]. Furthermore, no specific inhibitors exist for either UGGTs or EDEMs, so that assessment of the full impact of UGGT/EDEM modulation on the (glyco)secretome of cells with pharmacologically loosened ERQC/ERAD is challenging. Perhaps for these reasons, rescue of secretion of misfolded glycoprotein mutants by pharmacological UGGT/EDEM modulation has not been pursued and the molecular basis for the lack of secretion of glycoprotein mutants has been investigated only in a few cases [9,15,21,22].

Recently, the first sets of UGGT1 and UGGT2 client glycoproteins in HEK293 cells (the HEK293 "UGGT-omes" [19]) have been discovered [20], and a sub-millimolar inhibitor of both isoforms described [29], paving the way for investigation of the cellular consequences of UGGT modulation. The only rescue-of-secretion experiments of responsive glycoprotein mutants by UGGT KO published so far are the ones in plants, but ERQC/ERAD are well conserved in eukaryotes. We decided to test UGGT-based, broad-spectrum rescue-of-secretion approach for the first time in mammalian cells by evaluating the localisation of GDLD-associated Trop-2 glycoprotein mutants. Rescue of residual biological function carried by the Trop-2 mutants was also assessed in responsive colorectal cancer cells upon *UGGT1* inhibition.

Plasma membrane localisation of WT Trop-2 does not appear to depend on the presence of either UGGT isoforms: the WT glycoprotein reaches the cell membrane in all cell lines

tested, with no statistical differences observed in the degree of co-localisation with a plasma membrane marker. In contrast to WT Trop-2, the Trop-2-Q118E mutant glycoprotein does not reach the plasma membrane in *UGGT1*$^{+/+}$ cells. Lack of secretion likely underpins the GDLD associated with the mutation. Rescue of secretion of the same mutant in the *UGGT1*$^{-/-}$ and *UGGT1/2*$^{-/-}$cell lines suggests a role for UGGT1in recognising a folding defect of the Trop-2 mutant. Complementation of the *UGGT1*$^{-/-}$ and *UGGT1/2*$^{-/-}$cell lines with a WT *UGGT1* gene reverts the phenotype to the lack of secretion observed in the *UGGT1*$^{+/+}$ cells, while complementation of the same with an inactive *UGGT1* mutant still shows rescue of secretion of the misfolded Trop-2 mutant. These data support the hypothesis that UGGT1 activity is the source of ER retention of the mutant seen in the *UGGT1*$^{+/+}$ cells.

In order to confirm that the rescue of secretion observed in the *UGGT1*$^{-/-}$ background is due to Trop-2-Q118E mutant glycoprotein being a client of UGGT1 (and not to an indirect effect of the *UGGT1* KO) we went on to test *in cellula* glucosylation of Trop-2-Q118E. Our results confirm that Trop-2-Q118E is indeed a UGGT1 client. In our experiments, retention of the Trop-2-Q118E glycoprotein mutant in *UGGT2*$^{-/-}$ cells appears statistically equivalent to the WT one, but rescue of secretion in the *UGGT1/2*$^{-/-}$cells is slightly improved over the one observed in the *UGGT1*$^{-/-}$ background. These data may suggest a role for UGGT2 in the recognition of the defect in Trop-2-Q118E and/or in the folding of glycoproteins that mediate ER retention of the mutant. Indeed, glucosylation of the Trop-2-Q118E glycoprotein mutant by UGGT2 is also detectable *in cellula*, albeit at much reduced levels when compared with UGGT1-mediated glucosylation.

Despite the molecular determinants underpinning misfold-recognition by UGGT remaining elusive yet, it is currently hypothesised that the enzyme recognises and binds to misfolded glycoproteins through specific structural features, such as hydrophobic patches exposed on the protein surface due to incorrect folding. Using MD simulations we found that the Q118E mutation induces a disruption of the Trop-2 fold, likely due to an electrostatic repulsion between D107 and the sidechain of E118. This would result in a loss of the overall stability of the protein and transform the mutant glycoprotein into a substrate for UGGT. Membrane inserted Trop-2 is a dimer in which each monomer has five intramolecular disulphide bridges. Our Western blots of intermolecular SS-bonded Trop-2 multimers detect higher occurrences of Cys mispairing in the Q118E mutant. Q118 is flanked by the C119-C125 disulphide bridge, and the Q118E mutation may indeed disturb its formation. Consistent with this evidence, our flow cytometry experiments carried out using anti Trop-2 antibodies show that a large fraction of the Q118E mutant whose secretion is rescued in *UGGT*$^{-/-}$cells does not fold properly. Indeed, none of the Trop-2 Q118E, E227K and L186P mutants whose secretion is rescued by UGGT1 KO seems to carry residual Trop-2 activity.

The overall scope of ERQC/ERAD modulation for the therapy of such patients is yet to be assessed. The fraction of rare disease patients carrying a mild missense mutation in a secreted glycoprotein gene is not known, and it varies for each glycoprotein/rare disease [62]. For example, in lysosomal storage diseases and cystic fibrosis, an estimated 15-20% and 70% of patients carry a responsive mutant, respectively [4]. Each of these patients' mutation is in principle amenable to pharmacological chaperone therapy, and therefore could profit from

rescue-of-secretion therapy by ERQC/ERAD modulation, as a broad-spectrum alternative to pharmacological chaperone therapy.

Broad-spectrum strategies being based on modulation of basic cellular functions justifiably raise concerns, and modulators of ERQC are no exception: UGGT modulators in particular could cause premature secretion of incompletely folded glycoproteins [19]. However, upon close scrutiny, a few observations offer arguments in favour of further exploration of the idea. First and foremost, *UGGT1*$^{-/+}$ heterozygous mice express only 50–60% of UGGT1 as compared to their UGGT1 WT littermate; yet, they are viable, fertile, develop normally, and do not reveal any obvious phenotypic alterations up to adulthood [23]. The question is how can this be?

Two important things to remember are that most glycoproteins do not need UGGT to fold and that in *UGGT1*$^{-/-}$ cells, UGGT2 is still fully active. The UGGT-ome (the set of glycoproteins that require UGGT1 or UGGT2 for their folding) obviously depends on tissue- and cell-type, glycoprotein synthesis load and absence/presence of ER stress. However, all glycoproteins carrying one or more newly synthesised *N*-linked glycan, after the first action of ER glucosidases I and II, carry at least one mono-glucosylated glycan ($Glc_1Man_9GlcNAc_2$) and can therefore bind to calnexin/calreticulin and the associated folding enzymes/chaperones. The more *N*-linked glycans on a folding glycoprotein, the higher the chance that no UGGT-mediated reglucosylation is needed in order for that glycoprotein to access the calnexin cycle assisted folding machinery. Indeed, the recent and only published characterisation of the UGGT-omes in HEK293 cells lists less than 100 WT glycoproteins, while all other glycoproteins in the secretory pathway of these cells may fold without the need for UGGT [20]. The same study revealed partial redundancy between UGGT1 and UGGT2: amongst UGGT clients, some glycoproteins are assisted in their folding by both UGGT isoforms, while others require one but not the other UGGT isoform to fold. This is the case of the Trop-2 mutants, which we demonstrated here to be clients of UGGT1 but not UGGT2. Thus, an isoform-selective UGGT modulator is expected to have fewer side effects than a non-selective one, because the UGGT isoform that is not inhibited can still work on its isoform-specific glycoprotein clients.

When it comes to future means of making UGGT modulators into therapeutics, three more observations are worth considering. Firstly, all glycoproteins have a half-life. A UGGT inhibitor for rescue of all copies of a rare disease-associated missense responsive mutant will minimise damage to host cell if administered for a time shorter than the half-life of all the other secreted glycoproteins. One example of such ERQC inhibitors already used in the clinic are molecules targeting ER glucosidases I and II, acting as broad-spectrum antivirals, and given in high-dose, short-time pulses [63]. Pharmacokinetics of any future UGGT modulators drug candidate will similarly aim at a dose timed strategy that rescues enough secretion (and activity) of the target missense response mutant to confer therapeutic benefits, while at the same time relying on healthy glycoproteins being successfully folded and secreted between doses. Secondly, to increase their efficacy, and reduce their toxicity, host-targeting broad-spectrum antivirals can be combined into synergistic drug cocktails that contain traditional virus-targeted antivirals [64]. It is conceivable that a combination of a selective rescue-of-secretion UGGT modulator with a mutant-specific pharmacological

chaperone could achieve (in the field of rare disease caused by a responsive missense mutation in a secreted glycoprotein gene) results equivalent to antiviral cocktails. Thirdly, in all cases in which a UGGT modulator could be conceivably administered in a tissue-targeted manner and be ameliorated by topical/localised treatment (for example by unguents, sprays or drops), systemic toxicity is much less of a concern. Examples are syndromes selectively affecting the epidermis, or exposed mucosae or the cornea [65].

All in all, for many patients, rescue-of-secretion therapy using a UGGT isoform-specific drug may not turn out to be as risky a strategy as it may sound at first. The work described here constitutes a proof-of-principle study, encouraging testing of modulators of ERQC, and adding to the ERAD modulation approach described in [56], towards the development of broad-spectrum rescue-of-secretion drugs for the therapy of congenital rare diseases associated with responsive glycoprotein mutants.

Material and Methods

Computational Methods

For the Molecular Dynamics (MD) simulations, we used with minor modifications the protocol described by [66]. We utilised as initial structure a model built from the crystal structures of the cis-dimer of the extracellular domain of human Trop-2 (PDB IDs 7PEE [44] and 7E5N [45]) including only eight residues from the transmembrane region.

Starting from each structure (wild type and mutant), we prepared the systems and performed three replicas of a 1 μs all-atom MD simulation, using the AMBER package [67]. For each system, all non-protein molecules (carbohydrates) were removed from the PDB-deposited structure. The systems were prepared with the tleap module from the AMBER package, using the ff19SB/OPC force fields for amino acid/water molecules, respectively [68]. Standard protonation states were assigned to titratable residues (Asp and Glu are negatively charged; Lys and Arg are positively charged). Histidine protonation was assigned by favouring for each residue the formation of hydrogen bonds. All disulphide bonds as reported by Sun et al [45] were enforced/preserved throughout. The complete protonated systems were then solvated by a truncated cubic box of OPC waters, ensuring that the distance between the biomolecule surface and the box limit was at least 10 Å.

Each system was first optimised using a conjugate gradient algorithm for 5,000 steps, followed by 150 ps-long constant volume MD equilibration, in which the first 100 ps were used to gradually raise the temperature of the system from 0 to 300 K. The heating was followed by a 300 ps-long constant temperature and constant pressure MD simulation, to equilibrate the system density. During these temperature- and density-equilibration processes, the protein C_α atoms were constrained by a 5 kcal/mol/Å force constant, using a harmonic potential centred at each atom's starting position. Next, a second equilibration MD of 500 ps was performed, in which the integration step was increased to 2 fs and the force constant for restrained C_αs was decreased to 2 kcal/mol/Å, followed by 10 ns-long MD simulation with no constraints. Finally, a 1μs-long MD simulation was carried out, with no constraints and the ‘Hydrogen Mass Repartition’ method, which allows an integration step of 4 fs [69].

All simulations were performed using the pmemd.cuda algorithm from the AMBER package [70]. Pressure and temperature were kept constant using the Monte-Carlo barostat and Langevin thermostats, respectively, using default coupling parameters. All simulations were performed with a 10 Å cutoff for nonbonded interactions, and periodic boundary conditions, using the Particle Mesh Ewald summation method for long-range electrostatic interactions. The SHAKE algorithm was applied to all hydrogen-containing bonds in all simulations with an integration step equal or higher than 2 fs. All trajectory processing and parameters calculations were performed with the CPPTRAJ[71] module of the AMBER package. Images of the molecules were prepared using the Visual Molecular Dynamics (VMD) program [72]. The plots were created using the Matplotlib Python library [73].

Cell culture conditions

HEK293T and Vero E6 were cultured in DMEM, high glucose, GlutaMAX™ media supplemented with 10% FBS and 1% Antibiotic-Antimycotic (AB/AM) (Thermo Fisher Scientific, Waltham, MA, USA). KM12SM cells were cultured in RPMI supplemented with 10% FBS, 1% non-essential aminoacids and 1% MEM vitamins. All cells were kept at 37°C in humidified atmosphere containing 5% CO_2.

Generation of *UGGT1*$^{-/-}$, *UGGT2*$^{-/-}$ and *UGGT1/2*$^{-/-}$ knock-out cell lines

HEK293T cells: *UGGT1*$^{-/-}$, *UGGT2*$^{-/-}$ and *UGGT1/2*$^{-/-}$ HEK293T cells were generated using the CRISPR/Cas9 system from Addgene (http://www.addgene.org/). The sequences for guide RNAs were obtained from http://tools.genome-engineering.org and https://www.addgene.org/pooled-library/zhang-human-gecko-v2/. Guides (UGGT1: 5'-*gctgatgaacctccaccaga*-3'; UGGT2: 5'-*gacggtcgccgcgtccaagt*-3') were synthesised by Microsynth AG (Switzerland). They were inserted into the lentiCRISPRv2-puro vector (Addgene 52961) using the BsmBI restriction site. The plasmids were transfected with Jet Prime (Polyplus) into HEK293T cells. For the generation of *UGGT1/2*$^{-/-}$double KO cells, *UGGT1*-KO cells were re-transfected with the lentiCRISPRv2-puro containing the *UGGT2* guide and pCDNA3 vector to confer geneticin resistance. Two days after transfection, the cell culture medium was supplemented with 2 μg/mL puromycin for selection of the *UGGT1*$^{-/-}$ and *UGGT2*$^{-/-}$clones or with 200 μg/mL geneticin for selection of *UGGT1/2*$^{-/-}$cells. Puromycin or geneticin-resistant clones were collected after 10 days and cultured complete medium. Lack of protein expression was confirmed by Western blotting.

Vero E6 cells: For the generation of the *UGGT1*$^{-/-}$ and *UGGT2*$^{-/-}$ KO Vero E6 cells (ATCC) we used the CRISPR/Cas9 system as described in [74]. *Chlorocebussabaeus (Cs)* UGGT1 primers (Fwd1 CACCGGTGGCGTGAGGAGGCCTC; Rev1 AAACTGAGGCCTCCTCACGCCACC; Fwd2 CACCGTGGCTGTTCTCCTCAGTAA; Rev2 AAACTTACTGAGGAGAACAGCCAC) and *Cs*UGGT2 primers (Fwd1 CACCGCTGAAACATCTGAATAGC; Rev1 AAACAGCTATTCAGATGTTTCAGC; Fwd2 CACCGTGATTCTCTATGCCGAATT; Rev2 AAACAATTCGGCATAGAGAATCAC) were designed based on the *C. sabaeus* genome and cloned into pSpCas9(BB)-2A-Puro (Addgene # 62988, a gift from Feng Zhang) following the protocol in [75]. Vero E6 cells were transfected with the pair of CRISPR plasmids at 40% confluency using the Lipofectamine

3000 system (Thermo Fisher Scientific). Puromycin selection was performed between days 3-6 of culture at 3 μg/mL. The culture was separated into single cells at day 10 and clones propagated. Knockouts were confirmed by PCR screening, western blotting and sequencing (data not shown).

KM12SM cells: *UGGT1*$^{-/-}$ KM12SM cells were generated using the CRISPR/Cas9 system from Addgene (http://www.addgene.org/). The sequence for the guide RNA targeting *UGGT1* (5'-*gctgatgaacctccaccaga*-3') was synthesised by Sigma-Aldrich, and then inserted into the lentiCRISPRv2-puro vector as described above. The recombinant plasmid was transfected into HEK293T cells together with the packaging plasmids pCMV-VSV-G (Addgene #8454, a gift from Robert A. Weinberg) and psPAX2 (Addgene #12260, a gift from Didier Trono) using the Lipofectamine 3000 system. After 2 days the culture supernatant containing the recombinant lentiviruses released from HEK293T into the medium was collected, filtered through 0.45 μm syringe filters and used to infect the target KM12SM cells using 8 μg/mL Polybrene. Two days after infection, the medium was supplemented with 3 μg/mL puromycin for selection of the *UGGT1*$^{-/-}$ cells. Puromycin-resistant clones were collected after 15 days and propagated in complete medium supplemented with puromycin. Lack of protein expression was then confirmed by Western blotting.

Generation of mutant Trop-2 plasmids

The mutant Trop-2 plasmids encoding Trop-2-Q118E, Trop-2-E227K and Trop-2-L186P were generated from a WT Trop-2 template plasmid [76] through site-directed mutagenesis using the Q5 Site-Directed Mutagenesis Kit from New England Biolabs. The primers employed for obtaining the mutant Trop-2 plasmids were as follows (point mutations are indicated in bold): T2Q118E.for (5'-caaggcgcgc**g**agtgcaaccag-3'), T2Q118E.rev (5'-aagcggccctcggggtcg-3'), T2E227K.for (5'-ctactacttc**a**agagggacatcaaggg-3'), T2E227K.rev (5'-gcggcatcgccgatatcc-3') T2L186P.for (5'-cgctatcggc**c**gcaccccaag-3'), and T2L186P.rev (5'-ctcgcggaagagccgcct-3').

Cloning of the WT and mutant Trop-2 cDNAs into the pEYFP-N1 mammalian expression vector

The generation of the recombinant Trop-2-EYFP fusion constructs was carried out as described in [77]. The human WT Trop-2 and the Trop-2-Q118E, Trop-2-E227K, and Trop-2-L186P mutant cDNAs [76] were amplified by PCR (primers: F' gcgatt**ctcgag**tccggtccgcgttcc-**XhoI** and R' gcgcc**ggtacc**aagctcggttcctttc-**KpnI**) and sub-cloned into the pEYFP-N1 vector (Clontech, OH, USA) for mammalian expression to give theTrop-2-pEYFP-N1, Trop-2-Q118E-pEYFP-N1, Trop-2-E227K-pEYFP-N1 and Trop-2-L186P-pEYFP-N1 plasmids.

UGGT1 plasmids

Human UGGT1-encoding cDNA was cloned into the pCDNA3.1/Zeo(+) mammalian expression vector by using NheI/AflII restriction enzyme cloning sites. Additional 5' (GCTAGCA) and 3' sequences (CTTAAG) were added to the cDNA to carry out the cloning procedure (GenScript, Piscataway, NJ, USA). The inactive UGGT1 D1454A variant

was generated with direct mutagenesis by GenScript. The sequences of the constructs are provided in the supplementary documentation.

Generation of the *UGGT1* and *UGGT1 D1454A* complemented HEK293T stable cell lines

For the generation of our complemented stable cell lines, WT and *UGGT1*$^{-/-}$ HEK293T cells were cultured in 6-well plates (Corning, NY, USA) with 500,000 cells/1.5 mL starting cell density in DMEM, high glucose, GlutaMAX™ media supplemented with 10% FBS without antibiotics. After 24 hours, the HEK293T cells were transfected with 1 μg UGGT1-pCDNA3.1/Zeo(+) or UGGT1-D1454A-pCDNA3.1/Zeo(+) construct using X-tremeGENE 9 DNA transfection reagent (Roche, Basel, Switzerland) following the manufacturer's instructions. Stable transfectants were obtained by one-week selection with 400 μg/mL Zeocin (InvivoGen Europe, France), followed by one-week selection with 200 μg/mL Zeocin. After three weeks of selection, the cells were plated for the complementation experiments.

Transient transfection with constructs for expression of WT and mutant Trop-2 fluorescent chimeras

HEK293T cells were cultured in 6-well plates with $0.8x10^6$ cells/1.5 mL starting cell density. After 24 hours, the HEK293T WT, *UGGT1*$^{-/-}$, *UGGT2*$^{-/-}$ and *UGGT1/2*$^{-/-}$ cells were transfected with 1 μg Trop-2-pEYFP-N1 or Trop-2-Q118E-pEYFP-N1 plasmids using the X-tremeGENE 9 DNA transfection reagent (Roche, Basel, Switzerland) following the manufacturer's instructions.

Vero E6 and KM12SM cells were cultured in 6-well plates (Corning, NY, USA). After 24 hours, the Vero E6 WT, *UGGT1*$^{-/-}$, *UGGT2*$^{-/-}$ and *UGGT1/2*$^{-/-}$ cells and the KM12SM WT and *UGGT1*$^{-/-}$ cells were transfected with 1 μg Trop-2-pEYFP-N1 or Trop-2-Q118E-pEYFP-N1 or Trop-2-E227K-pEYFP-N1 or Trop-2-L186P-pEYFP-N1 plasmids using Lipofectamine 3000. Untransfected cells were used as a negative control.

Confocal microscopy analysis of the Trop-2-transfected HEK293T and Vero E6 cell lines

For the confocal microscopy measurements, we used organelle-specific staining in live cells to visualise the cellular localisation of the EYFP-labelled Trop-2 proteins. All of the stock solutions were diluted in prewarmed phenol-red free DMEM high glucose medium. The ER-Tracker Red dye (BODIPY TR Glibenclamide) was used at 1 μM final concentration to mark the ER. To visualise the plasma membrane, we applied Wheat Germ Agglutinin, Alexa Fluor 555 Conjugate (Thermo Fisher Scientific, Waltham, MA, USA) at 5 μg/mL working concentration. After 15 min incubation at 37 °C, the supernatant was carefully replenished with prewarmed phenol red free, high glucose DMEM supplemented with 10% FBS. The nuclei were stained with NucBlue Live ReadyProbes Reagent (Thermo Fisher Scientific, Waltham, MA, USA) following the manufacturer's instructions. After staining, we performed live cell imaging using Leica TCS SP5 and Zeiss LSM980 Airyscan 2 microscopes located at the Leicester University College of Life Sciences Advanced Imaging Facility (AIF) and equipped with a plan-apochromat 63x/1.4 objective. For live imaging, cells were incubated at 37°C and under 5% CO_2. Images were acquired in confocal mode (pixel size 66 x 66 nm) using sequential channel settings to minimise bleed-through.

All confocal images were taken with the same settings and single optical sections were analysed. For imaging of fixed cells, after organelle staining, cells were fixed using 3.7% paraformaldehyde for 10 mins at 37°C. Quenching was performed using 50mM NH_4Cl for 10 mins at RT. Nuclei were counterstained with DAPI and cellular localisation of EYFP-labelled Trop-2 proteins was imaged using a Zeiss LSM800 Airyscan 2 microscope located at the University of Chieti Center for Advanced Science and Technology AIF and equipped with a plan-apochromat 63x/1.4 objective.

Analysis of the confocal microscopy images

For image analysis, we used the Zeiss ZEN 3.1 Blue edition (Zeiss, Jena, Germany) and Fiji (version: 2.0.0-rc-69/1.52b) image processing softwares[47]. Zeiss LSM980 Airyscan 2 system with the Zen Blue software allows us to minimise bleed-through from the multiple channels by using sequential imaging and better emission wavelength separation. All of the confocal images were taken with the same settings and single optical sections were analysed. To measure the Trop-2 protein colocalisation with the membrane dye, we performed multichannel intensity plot analysis by using Fiji image processing tools. A single line was drawn across the cells and the intensity profiles were measured by an intensity line plot tool macro for each channel (FILM Macro Toolsets, Imperial College London). The overlapping signals show the colocalisation of different channels.

To measure the Trop-2 signal intensity (EYFP) in the cellular membrane, multiple regions of interest (ROIs) were selected based on the plasma membrane staining using ImageJ 1.53t software. All data are presented as means ± SEM and analysed by using Kruskal Wallis multiple comparison test in GraphPad Prism 10.0.2 (GraphPad Software, San Diego, CA, USA). A probability value (p) less than 0.05 was considered significant.

Isolation of hydrophobic, membrane-associated proteins from HEK293T cells with CelLytic™ MEM Protein Extraction Kit

Cells transfected with Trop-2-pEYFP-N1 and Trop-2-Q118E-pEYFP-N1 were harvested 24 hrs post-transfection with 100 µL PBS containing 1mM EDTA and the cell suspensions centrifuged at 200 x g for 5 min. The separation of membrane and soluble proteins from the pellet was carried out with CelLytic™ MEM Protein Extraction Kit (Sigma-Aldrich, MO, USA) following the manufacturer's instructions.

Transient transfection of WT and *UGGT1*$^{-/-}$ KO HEK293F cell lines with Trop-2 expressing constructs

HEK293F cells were cultured in FreeStyle™ 293 Expression Medium (Thermo Fisher Scientific, MA, USA). The initial concentration of the culture was $0.5x10^6$ cells/mL in 50 mL media. Cells were kept in an orbital shaker incubator at 37 °C, 120 rpm and 5% CO_2. Twenty-four hrs later or when they reached the $1x10^6$ cells/mL concentration, the cells were transfected with 1 µg plasmid DNA per million cells using polyethylenimine (PEI) in 1:4 ratio respectively in the presence of 5 µM kifunensine. The DNA was diluted in 5 mL sterile PBS then the PEI was added to the PBS/DNA solution. After a 20 min incubation at room temperature, the cells were transfected with the mixture.

Western blot analysis of Trop-2 protein in various membrane fractions

Protein concentration was determined with Coomassie (Bradford) Protein Assay Kit (Thermo Fisher Scientific, MA, USA) to ensure that the same amount of protein sample was loaded in each lane. For the SDS-page, 4-12% NuPAGE™ Bis-Tris precast polyacrylamide protein gels were used with 1x NuPAGE™ MES SDS Running Buffer (Thermo Fisher Scientific, MA, USA). The samples were prepared with NuPAGE™ LDS Sample Buffer (4X) (Thermo Fisher Scientific, MA, USA) in the presence or absence of a reducing agent (NuPAGE™ Sample Reducing Agent (10X), Thermo Fisher Scientific, MA, USA) and denatured at 92 °C for 10 minutes. The proteins were transferred overnight onto methanol activated polyvinylidene difluoride membrane (PVDF, Sigma-Aldrich, MO, USA) in Transfer Buffer (25 mM Tris, 190 mM Glycine, 20% (v/v) methanol). After the transfer, the membrane was blocked with 1x TBST + 5% skimmed milk powder for 2 hrs at room temperature. The blocking was followed by multiple washing cycles with 1x TBST. Anti-GFP monoclonal (GF28R) primary antibody (Thermo Fisher Scientific, MA, USA) was applied with 1:3000 dilution factor in 1x TBST+5% skimmed milk powder for 1.5 hrs at room temperature. After the 1x TBST washing cycles, Goat anti-Mouse IgG (H+L) Secondary Antibody DyLight 800 4x PEG (Thermo Fisher Scientific, MA, USA) was applied with 1:10,000 dilution factor in 1x TBST + 5% skimmed milk powder for 1 hr at room temperature. The membrane was washed after the secondary antibody and LI-COR Odyssey device was used with Image Studio™ software (LI-COR Biosciences, NE, USA) for the detection.

Transfection of Trop-2-EYFP and Q118E mutant into *ALG6*$^{-/-}$ background cells

The generation of the *ALG6*$^{-/-}$, *ALG6/UGGT1*$^{-/-}$,*ALG6/UGGT2*$^{-/-}$ *ALG6/UGGT1/2*$^{-/-}$cells has been previously described [20]. For each cell line 1.5 x 10^6 cells were plated onto 6 cm plates and grown in DMEM (Sigma D5796) containing 10% FBS for 24 hr. The following day the cells were transfected with either the Trop-2-pEYFP-N1 or Trop-2-Q118E-pEYFP-N1 plasmids. Briefly, 4.8 μg of DNA was diluted in Opti-Mem™ (Gibco 31985070) to a total volume of 80 μL. In a separate tube 12 μL of PEI (Polyscience 24765), formulated at 1 mg/mL, was added to 68 μL of Opti-Mem™ and incubated at room temperature for 5 min. After incubation, the PEI containing solution was added to the diluted DNA and incubated for an additional 20 min at 25 °C. The entire 160 μL of PEI:DNA mixture was added drop wise to each plate. The cells were returned to the incubator and incubated for 24 hr at 37 °C and 5% CO_2.

Cellular glucosylation assay

Prior to harvesting, the media of transfected cells was removed and 1 mL of fresh media containing 500 μM DNJ (Cayman 21065) was added. The cells were incubated for 5 hr at 37 °C and 5% CO_2. Before lysis, the media was removed, and the cells were washed with 1 mL of cold PBS and placed on ice. 500 μL of lysis buffer (20 mM MES, 100 mM NaCl, 30 mM Tris pH 7.5, 0.5% Triton X-100) containing both protease inhibitor (Thermo 1861278) and 20 mM *N*-ethylmaleimide was added to each plate and scraped to remove the attached cells. The lysate was removed and shaken vigorously for 10 min at 4 °C before centrifuging for 10 min at 20,817 x g and 4 °C. The centrifuged lysate was transferred to a fresh tube

and normalised to 750 μL. To each normalised tube, 25 μL of glutathione resin (Cytiva 17075601) was added, and tubes were incubated for 1 hr at 4 °C under gentle rotation to pre-clear the samples.

During this time, the glutathione resin pre-incubated with either GST-CRT or GST-CRT(Y109A) was prepared [20]. For each sample, 50 μL of glutathione resin was equilibrated with lysis buffer. After equilibration, the resin was split into two and 50 μg of recombinant GST-CRT or GST-CRT(Y109A) was added to one of the two samples. The volume of each sample was brought up to 500 μL with lysis buffer before incubating for 3 hr under gentle agitation at 4 °C. After incubation, the beads were centrifuged at 950 x g at 4 °C for 5 min and washed twice with lysis buffer. The pre-cleared supernatant was also centrifuged at 950 x g at 4 °C for 5 min to pellet the resin. The pre-cleared sample was then divided: 150 μL (20%) into 600 μL of cold acetone for the whole cell lysate and 262.5 μL (35%) to the GST-CRT and GST-CRT(Y109A) tubes. 200 μL of lysis buffer was added to each CRT and CRT(Y109A) tube and left to mix gently overnight at 4 °C. The tubes containing the whole cell lysate were mixed vigorously and incubated at −20°C overnight. The next day the glutathione resin was centrifuged at 950 x g for 5 min at 4 °C and washed twice with 500 μl of lysis buffer without protease inhibitor. The acetone precipitated samples were centrifuged for 10 min at 20,817 x g and 4 °C to pellet the precipitated protein. The acetone was removed, and the samples were dried for 5 min at 65 °C. 40 μL of loading buffer (30 mM Tris-HCl pH 6.8, 9% SDS, 15% glycerol, 0.05% bromophenol blue) containing 100 mM dithiothreitol (Sigma D9779) was added to each tube and the samples were boiled for 10 mins. 15 μl of each sample was resolved by 9% SDS-PAGE and transferred to a PVDF membrane (Millipore IPFL00010) and blotted using an anti-EYFP antibody (Thermo MA5-15256) and an anti-mouse secondary antibody (LI-CORE 926-32210).

ImageJ was used to quantify the immunoblots. To determine the percentage of glucosylation the amount of protein found in the whole cell lysate (WCL), GST-CRT, and GST-CRT(Y109A) was first normalised by their input percentages. Any background from the GST-CRT(Y109A) was subtracted from the GST-CRT before being divided by the normalised protein found within the WCL and multiplied by 100. The resulting values represented the amount of WT or mutant Trop-2 glucosylated by UGGT.

Endoglycosidase Assay

The Trop-2-EYFP or the Trop-2-Q118E-EYFP mutant plasmid was transfected into HEK293, *ALG6*$^{-/-}$ or *UGGT1*$^{-/-}$ cells. The generation of the *ALG6*$^{-/-}$ and *UGGT1*$^{-/-}$ cell lines have been detailed elsewhere [20]. For each cell line, 7.5x105 cells were plated onto a 3-cm dish and grown for 24 hr at 37 °C and 5% CO_2 before transfecting. After transfection, the cells were harvested and the lysates were processed as described earlier. The clarified lysates were then divided: 30% (90 μL) for a non-treated sample, 30% (90 μL) for PNGaseF digestion (NEB P0705S) and 30% (90 μL) for EndoH digestion (NEB P0702S).

Preparation of each digestion sample was done according to the manufacturer's recommendations. Briefly, the protocol was scaled to 90 μL and the corresponding volumes of water and denaturation buffer were added to each tube. The samples were then treated at 100 °C for 10 min. Glycobuffer 2 and 10% NP40 were added to the non-treated and

PNGaseF samples, while Glycobuffer 3 was added to the EndoH sample. Finally, 1 μL of PNGaseF and EndoH were added to the corresponding tubes while 1 μL of water was added to the non-treated condition. The samples were rotated end-over-end overnight at 37 °C. The next day the samples were mixed with 500 μL of cold acetone and incubated at −20°C for at least 5 hr. After incubation the samples were centrifuged for 10 min at 20,817 x g, 4 °C before the supernatant was removed. The pellets were dried overnight at 25 °C before being resuspended the next day with 30 μL of loading buffer containing 100 mM dithiothreitol. Each tube was heated at 100 °C for 10 min and shaken vigorously for 10 min. 25 μL of each sample was resolved by 9% SDS-PAGE, transferred to a PVDF membrane, and blotted using the same anti-EYFP used for the glucosylation assay.

Flow cytometry analysis of membrane-recruited WT and Q118E Trop-2 mutants

UGGT1$^{-/-}$Vero E6 cells transfected with Trop-2-pEYFP-N1 or Trop-2-Q118E-pEYFP-N1 plasmid were stained after 48 hrs for flow cytometry. An anti Trop-2 mAb (T16) or anti Trop-2 pAb (AF650 from R&D Systems) was used to perform staining of live, non-permeabilised cells. The secondary antibodies were APC-labelled Donkey anti mouse (for binding to T16) or Donkey anti Goat (for binding to pAb) and were utilised for secondary staining of the cells after removal of the primary antibodies with 3 washes using PBS. Fluorescent signals in the EYFP and in the APC channels were acquired for subsequent evaluation of the MFIs.

Cell proliferation assay

UGGT1$^{+/+}$ and *UGGT1*$^{-/-}$KM12SM cells were transfected with EYFP, WT Trop-2-EYFP or Trop-2-Q118E-EYFP. At 48 hrs after transfection, cells were seeded in triplicate in 96-well optical-bottom plates. At 4 hrs (time = 0) and 28 hrs (time = 24 hrs) after seeding, the number of fluorescent cells was obtained by fluorescence/confocal microscopy imaging of the whole wells (tile-imaging acquisition using a 20x objective) and quantification of the fluorescence images using the following ImageJ/Fiji procedure: Image → Adjust → Auto Threshold → Method (Yen) → Analyze → Analyse Particles → Size = (2-infinity). For each well a number was obtained, and then the number of the cells for each experimental group was retrieved by computing the average of the triplicate values.

Imaging analysis of intracellular calcium levels

UGGT1$^{+/+}$ and *UGGT1*$^{-/-}$ KM12SM cells were transfected with WT Trop-2-EYFP, Trop-2-Q118E-EYFP, Trop-2-E227K-EYFP or Trop-2-L186P-EYFP. Co-transfection of these EYFP chimeras with a red fluorescent genetically encoded calcium indicator (CMV-R-GECO1.2) was carried out in order to assess the potential increase of the intracellular Ca^{2+} levels by confocal, time-lapse fluorescence microscopy, as described in [32]. Stitching of 7-sec timeframes was carried out through the ImageJ/Fiji “Montage” command.

Supplementary Material

Refer to Web version on PubMed Central for supplementary material.

Acknowledgments:

P.R. and M.T. are supported by the Cariplo-Telethon Alliance, grant reference GJC22077A. P.R. was the recipient of a LISCB Wellcome Trust ISSF award, grant reference 204801/Z/16/Z. M.T. was supported by the Italian Ministry of University and Research, Programma Per Giovani Ricercatori “Rita Levi Montalcini” grant reference PGR12I7N1Z. G.T. was funded by a Wellcome Trust Seed Award in Science to P.R., grant reference 214090/Z/18/Z. A.L. was the recipient of an Italian Government PhD Studentship. M.M. is supported by Signora Alessandra, AlphaONE Foundation, Foundation for Research on Neurodegenerative Diseases, Swiss National Science Foundation, Comel and Gelu Foundations. We thank the Advanced Imaging Facility (RRID:SCR_020967) at the University of Leicester for support. The Zeiss LSM 980 Airyscan 2 system was funded by a BBSRC grant for the Advanced Imaging Facility (AIF), reference number BB/S019510/1. This work was also supported by the National Institutes of Health (GM086874 to D.N.H.) and a Chemistry-Biology Interface program training grant (T32 GM139789 to K.P.G.). Feng Xhang donated the pSpCas9(BB)-2A-Puro vector. Robert A. Weinberg donated the pCMV-VSV-G vector. Didier Trono donated the psPAX2 vector. Siyu Wang and Louise Fairall helped with HEK293F cell expression. Michelle Hill assisted us in the generation of the Vero E6 KO cell lines. N.Z. is a Fellow of Merton College Oxford.

References

1. Adams BM, Oster ME, and Hebert DN (2019). Protein Quality Control in the Endoplasmic Reticulum. Protein J. 38, 317–329. [PubMed: 31004255]
2. Klausner RD, and Sitia R (1990). Protein degradation in the endoplasmic reticulum. Cell 62, 611–614. [PubMed: 2201450]
3. Wiseman RL, Mesgarzadeh JS, and Hendershot LM (2022). Reshaping endoplasmic reticulum quality control through the unfolded protein response. Mol. Cell 82, 1477–1491. [PubMed: 35452616]
4. Parenti G, Andria G, and Valenzano KJ (2015). Pharmacological Chaperone Therapy: Preclinical Development, Clinical Translation, and Prospects for the Treatment of Lysosomal Storage Disorders. Mol. Ther 23, 1138–1148. [PubMed: 25881001]
5. Marinko JT, Huang H, Penn WD, Capra JA, Schlebach JP, and Sanders CR (2019). Folding and Misfolding of Human Membrane Proteins in Health and Disease: From Single Molecules to Cellular Proteostasis. Chem. Rev 119, 5537–5606. [PubMed: 30608666]
6. Annoni A, Gregori S, Naldini L, and Cantore A (2019). Modulation of immune responses in lentiviral vector-mediated gene transfer. Cell. Immunol 342, 103802. [PubMed: 29735164]
7. Schaible P. (2023). Modifying enzyme replacement therapy - A perspective. J. Cell. Mol. Med 27, 165–173. [PubMed: 36566487]
8. Amara JF, Cheng SH, and Smith AE (1992). Intracellular protein trafficking defects in human disease. Trends Cell Biol. 2, 145–149. [PubMed: 14731969]
9. Merulla J, Soldà T, and Molinari M (2015). A novel UGGT1 and p97-dependent checkpoint for native ectodomains with ionizable intramembrane residue. Mol. Biol. Cell 26, 1532–1542. [PubMed: 25694454]
10. Jin H, Yan Z, Nam KH, and Li J (2007). Allele-specific suppression of a defective brassinosteroid receptor reveals a physiological role of UGGT in ER quality control. Mol. Cell 26, 821–830. [PubMed: 17588517]
11. Hüttner S, Veit C, Vavra U, Schoberer J, Liebminger E, Maresch D, Grass J, Altmann F, Mach L, and Strasser R (2014). Arabidopsis Class I α-Mannosidases MNS4 and MNS5 Are Involved in Endoplasmic Reticulum-Associated Degradation of Misfolded Glycoproteins. Plant Cell 26, 1712–1728. [PubMed: 24737672]
12. Soheili T, Gicquel E, Poupiot J, N’Guyen L, Le Roy F, Bartoli M, and Richard I (2012). Rescue of sarcoglycan mutations by inhibition of endoplasmic reticulum quality control is associated with minimal structural modifications. Hum. Mutat 33, 429–439. [PubMed: 22095924]
13. Roversi P, Marti L, Caputo AT, Alonzi DS, Hill JC, Dent KC, Kumar A, Levasseur MD, Lia A, Waksman T, et al. (2017). Interdomain conformational flexibility underpins the activity of UGGT, the eukaryotic glycoprotein secretion checkpoint. Proceedings of the National Academy of Sciences 114, 8544–8549.

14. Pearse BR, Tamura T, Sunryd JC, Grabowski GA, Kaufman RJ, and Hebert DN (2010). The role of UDP-Glc:glycoprotein glucosyltransferase 1 in the maturation of an obligate substrate prosaposin. J. Cell Biol 189, 829–841. [PubMed: 20498017]
15. Molinari M, Galli C, Vanoni O, Arnold SM, and Kaufman RJ (2005). Persistent glycoprotein misfolding activates the glucosidase II/UGT1-driven calnexin cycle to delay aggregation and loss of folding competence. Mol. Cell 20, 503–512. [PubMed: 16307915]
16. Pankow S, Bamberger C, Calzolari D, Martínez-Bartolomé S, Lavallée-Adam M, Balch WE, and Yates JR 3rd (2015). ΔF508 CFTR interactome remodelling promotes rescue of cystic fibrosis. Nature 528, 510–516. [PubMed: 26618866]
17. Ritter C, and Helenius A (2000). Recognition of local glycoprotein misfolding by the ER folding sensor UDP-glucose:glycoprotein glucosyltransferase. Nat. Struct. Biol 7, 278–280. [PubMed: 10742170]
18. Labriola C, Cazzulo JJ, and Parodi AJ (1999). Trypanosoma cruzi calreticulin is a lectin that binds monoglucosylated oligosaccharides but not protein moieties of glycoproteins. Mol. Biol. Cell 10, 1381–1394. [PubMed: 10233151]
19. Tax G, Lia A, Santino A, and Roversi P (2019). Modulation of ERQC and ERAD: A Broad-Spectrum Spanner in the Works of Cancer Cells? J. Oncol 2019, 8384913. [PubMed: 31662755]
20. Adams BM, Canniff NP, Guay KP, Larsen ISB, and Hebert DN (2020). Quantitative glycoproteomics reveals cellular substrate selectivity of the ER protein quality control sensors UGGT1 and UGGT2. Elife 9. 10.7554/eLife.63997.
21. Soldà T, Galli C, Kaufman RJ, and Molinari M (2007). Substrate-specific requirements for UGT1-dependent release from calnexin. Mol. Cell 27, 238–249. [PubMed: 17643373]
22. Tannous A, Patel N, Tamura T, and Hebert DN (2015). Reglucosylation by UDP-glucose:glycoprotein glucosyltransferase 1 delays glycoprotein secretion but not degradation. Mol. Biol. Cell 26, 390–405. [PubMed: 25428988]
23. Huang P-N, Jheng J-R, Arnold JJ, Wang J-R, Cameron CE, and Shih S-R (2017). UGGT1 enhances enterovirus 71 pathogenicity by promoting viral RNA synthesis and viral replication. PLoSPathog. 13, e1006375.
24. Trombetta ES, and Helenius A (1999). Glycoprotein reglucosylation and nucleotide sugar utilization in the secretory pathway: identification of a nucleoside diphosphatase in the endoplasmic reticulum. EMBO J. 18, 3282–3292. [PubMed: 10369669]
25. Abe J, Takeda Y, Kikuma T, Kizuka Y, Kajiura H, Kajihara Y, and Ito Y (2023). Squaryl group-modified UDP analogs as inhibitors of the endoplasmic reticulum-resident folding sensor enzyme UGGT. Chem. Commun 59, 2803–2806.
26. Kudo T, Hirano M, Ishihara T, Shimura S, and Totani K (2014). Glycopeptide probes for understanding peptide specificity of the folding sensor enzyme UGGT. Bioorganic & Medicinal Chemistry Letters 24, 5563–5567. 10.1016/j.bmcl.2014.11.013. [PubMed: 25466175]
27. Totani K, Ihara Y, Tsujimoto T, Matsuo I, and Ito Y (2009). The recognition motif of the glycoprotein-folding sensor enzyme UDP-Glc:glycoprotein glucosyltransferase. Biochemistry 48, 2933–2940. [PubMed: 19222173]
28. Caputo AT, Ibba R, Le Cornu JD, Darlot B, Hensen M, Lipp CB, Marcianò G, Vasiljević S, Zitzmann N, and Roversi P (2022). Crystal polymorphism in fragment-based lead discovery of ligands of the catalytic domain of UGGT, the glycoprotein folding quality control checkpoint. Front Mol Biosci9, 960248. [PubMed: 36589243]
29. Guay KP, Ibba R, Kiappes JL, Vasiljević S, Bonì F, De Benedictis M, Zeni I, Le Cornu JD, Hensen M, Chandran AV, et al. (2023). A quinolin-8-ol sub-millimolar inhibitor of UGGT, the ER glycoprotein folding quality control checkpoint. iScience26, 107919. [PubMed: 37822503]
30. Guerra E, Trerotola M, Tripaldi R, and Aloisi AL (2016). Trop-2 Induces Tumor Growth Through AKT and Determines Sensitivity to AKT InhibitorsAKT Is a Downstream Effector of Trop-2. Cancer Res.
31. Trerotola M, Guerra E, Ali Z, Aloisi AL, Ceci M, Simeone P, Acciarito A, Zanna P, Vacca G, D'Amore A, et al. (2021). Trop-2 cleavage by ADAM10 is an activator switch for cancer growth and metastasis. Neoplasia 23, 415–428. [PubMed: 33839455]

32. Guerra E, Relli V, Ceci M, Tripaldi R, Simeone P, Aloisi AL, Pantalone L, La Sorda R, Lattanzio R, Sacchetti A, et al. (2022). Trop-2, Na+/K+ ATPase, CD9, PKCα, cofilin assemble a membrane signaling super-complex that drives colorectal cancer growth and invasion. Oncogene 41, 1795–1808. [PubMed: 35132180]
33. Guerra E, Trerotola M, Relli V, Lattanzio R, Tripaldi R, Ceci M, Boujnah K, Pantalone L, Sacchetti A, Havas KM, et al. (2023). 3D-informed targeting of the Trop-2 signal-activation site drives selective cancer vulnerability. Mol. Cancer Ther 10.1158/1535-7163.MCT-22-0352.
34. Tsujikawa M, Kurahashi H, Tanaka T, Nishida K, Shimomura Y, Tano Y, and Nakamura Y (1999). Identification of the gene responsible for gelatinous drop-like corneal dystrophy. Nat. Genet 21, 420–423. [PubMed: 10192395]
35. Alavi A, Elahi E, Tehrani MH, Amoli FA, Javadi M-A, Rafati N, Chiani M, Banihosseini SS, Bayat B, Kalhor R, et al. (2007). Four mutations (three novel, one founder) in TACSTD2 among Iranian GDLD patients. Invest. Ophthalmol. Vis. Sci 48, 4490–4497. [PubMed: 17898270]
36. Fujiki K, Nakayasu K, and Kanai A (2001). Corneal dystrophies in Japan. J. Hum. Genet 46, 431–435. [PubMed: 11501939]
37. Nakaizumi G. (1914). A rare case of corneal dystrophy (in Japanese). J JpnOphthalmol Soc 18, 949–950.
38. Ren Z, Lin P-Y, Klintworth GK, Iwata F, Munier FL, Schorderet DF, El Matri L, Theendakara V, Basti S, Reddy M, et al. (2002). Allelic and locus heterogeneity in autosomal recessive gelatinous drop-like corneal dystrophy. Hum. Genet 110, 568–577. [PubMed: 12107443]
39. Kawasaki S, and Kinoshita S (2011). Clinical and Basic Aspects of Gelatinous Drop-Like Corneal Dystrophy. In, pp. 97–115.
40. Nagahara Y, Tsujikawa M, Koto R, Uesugi K, Sato S, Kawasaki S, Maruyama K, and Nishida K (2020). Corneal Opacity Induced by Light in a Mouse Model of Gelatinous Drop-Like Corneal Dystrophy. Am. J. Pathol 190, 2330–2342. [PubMed: 33011110]
41. Tsujikawa M. (2012). Gelatinous Drop–Like Corneal Dystrophy. Cornea 31, S37. [PubMed: 23038033]
42. Mirdita M, Schütze K, Moriwaki Y, Heo L, Ovchinnikov S, and Steinegger M (2022). ColabFold: making protein folding accessible to all. Nat. Methods 19, 679–682. [PubMed: 35637307]
43. Webb B, and Sali A (2016). Comparative Protein Structure Modeling Using MODELLER. Curr. Protoc. Bioinformatics 54, 5.6.1–5.6.37.
44. Pavšič M. (2021). Trop2 Forms a Stable Dimer with Significant Structural Differences within the Membrane-Distal Region as Compared to EpCAM. Int. J. Mol. Sci 22. 10.3390/ijms221910640.
45. Sun M, Zhang H, Jiang M, Chai Y, Qi J, Gao GF, and Tan S (2021). Structural insights into the cis and trans assembly of human trophoblast cell surface antigen 2. iScience24, 103190. [PubMed: 34693228]
46. Paul D, Stern O, Vallis Y, Dhillon J, Buchanan A, and McMahon H (2023). Cell surface protein aggregation triggers endocytosis to maintain plasma membrane proteostasis. Nat. Commun 14, 947. [PubMed: 36854675]
47. Schindelin J, Arganda-Carreras I, Frise E, Kaynig V, Longair M, Pietzsch T, Preibisch S, Rueden C, Saalfeld S, Schmid B, et al. (2012). Fiji: an open-source platform for biological-image analysis. Nat. Methods 9, 676–682. [PubMed: 22743772]
48. Arnold SM, Fessler LI, Fessler JH, and Kaufman RJ (2000). Two Homologues Encoding Human UDP-Glucose:Glycoprotein Glucosyltransferase Differ in mRNA Expression and Enzymatic Activity. Biochemistry 39, 2149–2163. 10.1021/bi9916473. [PubMed: 10694380]
49. Satoh T, Song C, Zhu T, Toshimori T, Murata K, Hayashi Y, Kamikubo H, Uchihashi T, and Kato K (2017). Visualisation of a flexible modular structure of the ER folding-sensor enzyme UGGT. Sci. Rep 7, 12142. [PubMed: 28939828]
50. Aebi M. (2013). N-linked protein glycosylation in the ER. Biochim. Biophys. Acta 1833, 2430–2437. [PubMed: 23583305]
51. Kapoor M, Ellgaard L, Gopalakrishnapai J, Schirra C, Gemma E, Oscarson S, Helenius A, and Surolia A (2004). Mutational analysis provides molecular insight into the carbohydrate-binding region of calreticulin: pivotal roles of tyrosine-109 and aspartate-135 in carbohydrate recognition. Biochemistry43, 97–106. [PubMed: 14705935]

52. Alberti S, Miotti S, Stella M, Klein CE, Fornaro M, Menard S, and Colnaghi MI (1992). Biochemical characterization of Trop-2, a cell surface molecule expressed by human carcinomas: formal proof that the monoclonal antibodies T16 and MOv-16 recognize Trop-2. Hybridoma 11, 539–545. [PubMed: 1459581]
53. Zhao Y, Araki S, Wu J, Teramoto T, Chang Y-F, Nakano M, Abdelfattah AS, Fujiwara M, Ishihara T, Nagai T, et al. (2011). An expanded palette of genetically encoded Ca^{2+} indicators. Science 333, 1888–1891. [PubMed: 21903779]
54. Hebert DN, Lamriben L, Powers ET, and Kelly JW (2014). The intrinsic and extrinsic effects of N-linked glycans on glycoproteostasis. Nat. Chem. Biol 10, 902–910. [PubMed: 25325701]
55. Adams BM, Ke H, Gierasch LM, Gershenson A, and Hebert DN (2019). Proper secretion of the serpin antithrombin relies strictly on thiol-dependent quality control. J. Biol. Chem 294, 18992–19011. [PubMed: 31662433]
56. Henriques SF, Patissier C, Bourg N, Fecchio C, Sandona D, Marsolier J, and Richard I (2018). Different outcome of sarcoglycan missense mutation between human and mouse. PLoS One 13, e0191274. [PubMed: 29360879]
57. Kerem BS, Buchanan JA, Durie P, Corey ML, Levison H, Rommens JM, Buchwald M, and Tsui LC (1989). DNA marker haplotype association with pancreatic sufficiency in cystic fibrosis. Am. J. Hum. Genet 44, 827–834. [PubMed: 2567116]
58. Nilsson SC, Trouw LA, Renault N, Miteva MA, Genel F, Zelazko M, Marquart H, Muller K, Sjöholm AG, Truedsson L, et al. (2009). Genetic, molecular and functional analyses of complement factor I deficiency. Eur. J. Immunol 39, 310–323. [PubMed: 19065647]
59. Ben Bdira F, Kallemeijn WW, Oussoren SV, Scheij S, Bleijlevens B, Florea BI, van Roomen CPAA, Ottenhoff R, van Kooten MJFM, Walvoort MTC, et al. (2017). Stabilization of Glucocerebrosidase by Active Site Occupancy. ACS Chem. Biol 12, 1830–1841. [PubMed: 28485919]
60. Tucker JD, Lu PJ, Xiao X, and Lu QL (2018). Overexpression of Mutant FKRP Restores Functional Glycosylation and Improves Dystrophic Phenotype in FKRP Mutant Mice. Mol. Ther. Nucleic Acids 11, 216–227. [PubMed: 29858056]
61. Beerepoot P, Nazari R, and Salahpour A (2017). Pharmacological chaperone approaches for rescuing GPCR mutants: Current state, challenges, and screening strategies. Pharmacol. Res 117, 242–251. [PubMed: 28027910]
62. Cheng J, Novati G, Pan J, Bycroft C, Žemgulytė A, Applebaum T, Pritzel A, Wong LH, Zielinski M, Sargeant T, et al. (2023). Accurate proteome-wide missense variant effect prediction with AlphaMissense. Science 381, eadg7492. [PubMed: 37733863]
63. Dwek RA, Bell JI, Feldmann M, and Zitzmann N (2022). Host-targeting oral antiviral drugs to prevent pandemics. Lancet 399, 1381–1382. [PubMed: 35344736]
64. Oksenych V, and Kainov DE (2022). Broad-Spectrum Antivirals and Antiviral Drug Combinations. Viruses 14. 10.3390/v14020301.
65. Kaza H, Barik MR, Reddy MM, Mittal R, and Das S (2017). Gelatinous drop-like corneal dystrophy: a review. Br. J. Ophthalmol 101, 10–15. [PubMed: 27913443]
66. Modenutti CP, Blanco Capurro JI, Ibba R, Alonzi DS, Song MN, Vasiljević S, Kumar A, Chandran AV, Tax G, Marti L, et al. (2021). Clamping, bending, and twisting inter-domain motions in the misfold-recognizing portion of UDP-glucose: Glycoprotein glucosyltransferase. Structure 29, 357–370.e9. [PubMed: 33352114]
67. Case DA, MetinAktulga H, Belfon K, Ben-Shalom I, Berryman JT, Brozell SR, Cerutti DS, Cheatham TE III, Andrés Cisneros G, Cruzeiro VWD, et al. (2022). Amber 2022 (University of California, San Francisco).
68. Tian C, Kasavajhala K, Belfon KAA, Raguette L, Huang H, Migues AN, Bickel J, Wang Y, Pincay J, Wu Q, et al. (2020). ff19SB: Amino-Acid-Specific Protein Backbone Parameters Trained against Quantum Mechanics Energy Surfaces in Solution. J. Chem. Theory Comput 16, 528–552. [PubMed: 31714766]
69. Hopkins CW, Le Grand S, Walker RC, and Roitberg AE (2015). Long-Time-Step Molecular Dynamics through Hydrogen Mass Repartitioning. J. Chem. Theory Comput 11, 1864–1874. [PubMed: 26574392]

70. Salomon-Ferrer R, Götz AW, Poole D, Le Grand S, and Walker RC (2013). Routine Microsecond Molecular Dynamics Simulations with AMBER on GPUs. 2. Explicit Solvent Particle Mesh Ewald. J. Chem. Theory Comput 9, 3878–3888. [PubMed: 26592383]

71. Roe DR, and Cheatham TE 3rd (2013). PTRAJ and CPPTRAJ: Software for Processing and Analysis of Molecular Dynamics Trajectory Data. J. Chem. Theory Comput 9, 3084–3095. [PubMed: 26583988]

72. Humphrey W, Dalke A, and Schulten K (1996). VMD: visual molecular dynamics. J. Mol. Graph 14, 33–38, 27–28. [PubMed: 8744570]

73. Hunter JD (2007). Matplotlib: A 2D Graphics Environment. Comput. Sci. Eng 9, 90–95.

74. Bauer DE, Canver MC, and Orkin SH (2015). Generation of genomic deletions in mammalian cell lines via CRISPR/Cas9. J. Vis. Exp, e52118. [PubMed: 25549070]

75. Ran FA, Hsu PD, Wright J, Agarwala V, Scott DA, and Zhang F (2013). Genome engineering using the CRISPR-Cas9 system. Nat. Protoc 8, 2281–2308. [PubMed: 24157548]

76. Fornaro M, Dell'Arciprete R, Stella M, Bucci C, Nutini M, Capri MG, and Alberti S (1995). Cloning of the gene encoding Trop-2, a cell-surface glycoprotein expressed by human carcinomas. Int. J. Cancer 62, 610–618. [PubMed: 7665234]

77. Trerotola M, Li J, Alberti S, and Languino LR (2012). Trop-2 inhibits prostate cancer cell adhesion to fibronectin through the β1 integrin-RACK1 axis. J. Cell. Physiol 227, 3670–3677. [PubMed: 22378065]

Synopsis:

Deletion of the *UGGT1* gene in mammalian cells rescues secretion of fluorescent chimeras of the human Trop-2 Q118E, E227K and L186P glycoprotein mutants, which are associated to gelatinous drop-like corneal dystrophy. These mutants are retained in the secretory pathway in $UGGT1^{+/+}$ wild type cells and they localise to the plasma membrane in $UGGT1^{-/-}$knock-out cells. The Trop-2-Q118E glycoprotein disease mutant is efficiently glucosylated by UGGT1 in human cells demonstrating that it is a *bona fide* cellular UGGT1 substrate.

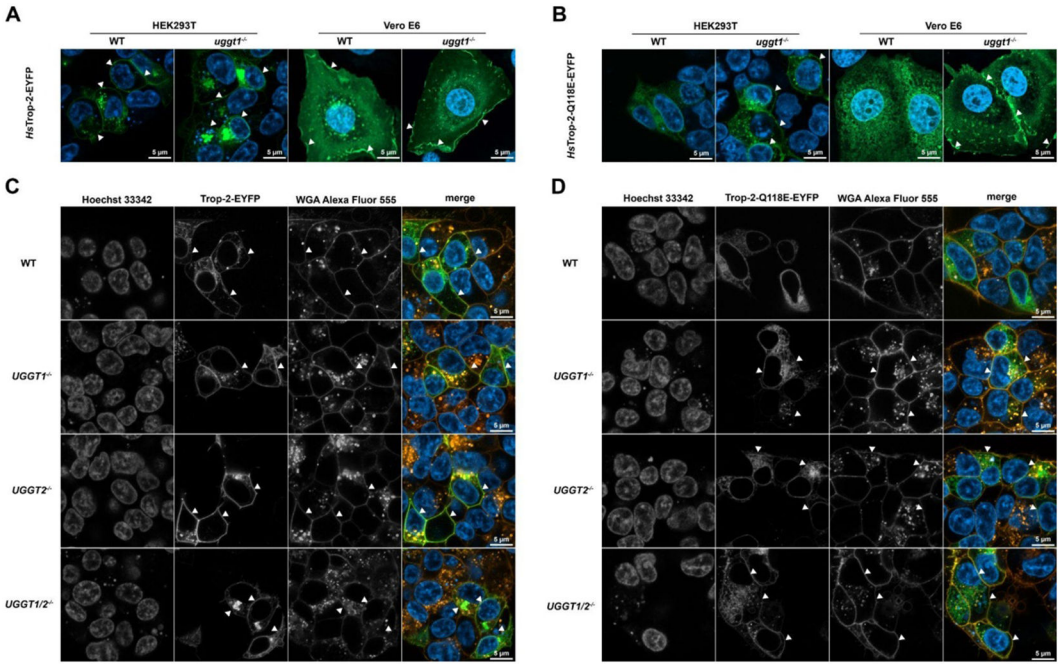

Figure 1. Rescue of secretion of the Trop-2-Q118E-EYFP- mutant glycoprotein upon UGGT1 inactivation.

Confocal images of single optical sections of transiently transfected HEK293T (live imaging) and Vero E6 cells (fixed cells).Nuclei were stained with Hoechst 33342 in HEK293T cells or with DAPI stain in Vero E6 cells (blue). **(A, B):** Wild type (WT) and *UGGT1*$^{-/-}$HEK293T and Vero E6 cells were transiently transfected with Trop-2-pEYFP-N1 and Trop-2-Q118E-pEYFP-N1 plasmids. **(A):** The Trop-2-EYFP wild type glycoprotein (green) traverses the secretory pathway and reaches the plasma membrane (white arrowheads);**(B)**: in WT cells, the Trop-2-Q118E-EYFP mutant glycoprotein (green) is visible in the secretory pathway but absent from the plasma membrane. In the *UGGT1*$^{-/-}$ cells, the same Trop-2-Q118E-EYFP mutant glycoprotein reaches the cellular membrane (white arrowheads). **(C, D)** WT, *UGGT1*$^{-/-}$, *UGGT2*$^{-/-}$, and *UGGT1/2*$^{-/-}$HEK293T cells were transiently transfected with Trop-2-pEYFP-N1 **(C)** and Trop-2-Q118E-pEYFP-N1 plasmids **(D)**. Wheat Germ Agglutinin (WGA) Alexa Fluor 555 (orange) enables verification of plasma membrane localisation of the fluorescent fusion glycoproteins; **(C):** in both WT and *UGGT1*$^{-/-}$ HEK293T cells the Trop-2-EYFP-WT glycoprotein (green) reaches the cellular membrane (white arrowheads); **(D):** in the WT HEK293T cells the Trop-2-Q118E-EYFP mutant glycoprotein (green) is trapped in the secretory pathway, while in the *UGGT1*$^{-/-}$and *UGGT1/2*$^{-/-}$HEK293T cells (and to a lower extent in *UGGT2*$^{-/-}$ cells) the same mutant glycoprotein is visible both in the ER and in the membrane (white arrowheads).

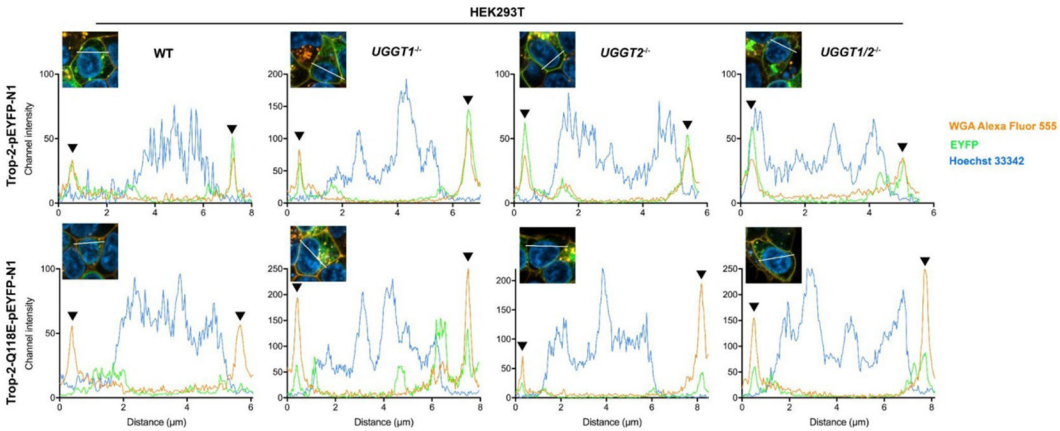

Figure 2. Multichannel intensity plots of the Trop-2-pEYFP-N1 transfected HEK293T cell lines.

For each combination of cell line and transiently transfected vector, the fluorescent signal is plotted along the line drawn in white in the inset panel. Labelling: green = EYFP; orange = WGA Alexa Fluor 555; blue = Hoechst 33342. The signal from the WGA Alexa Fluor 555 labelled membrane (orange) overlaps with EYFP (green) signals in Trop-2-pEYFP-N1 transfected cells (black arrowheads, top row). In the case of the mutant Trop-2-Q118E-pEYFP-N1 transfected cells, the protein is absent from the membrane in WT cells (bottom left panel). The deletion of one or both *UGGT* genes rescues secretion of the misfolded Trop-2 mutant glycoprotein (black arrowheads, all bottom panels but the leftmost one).

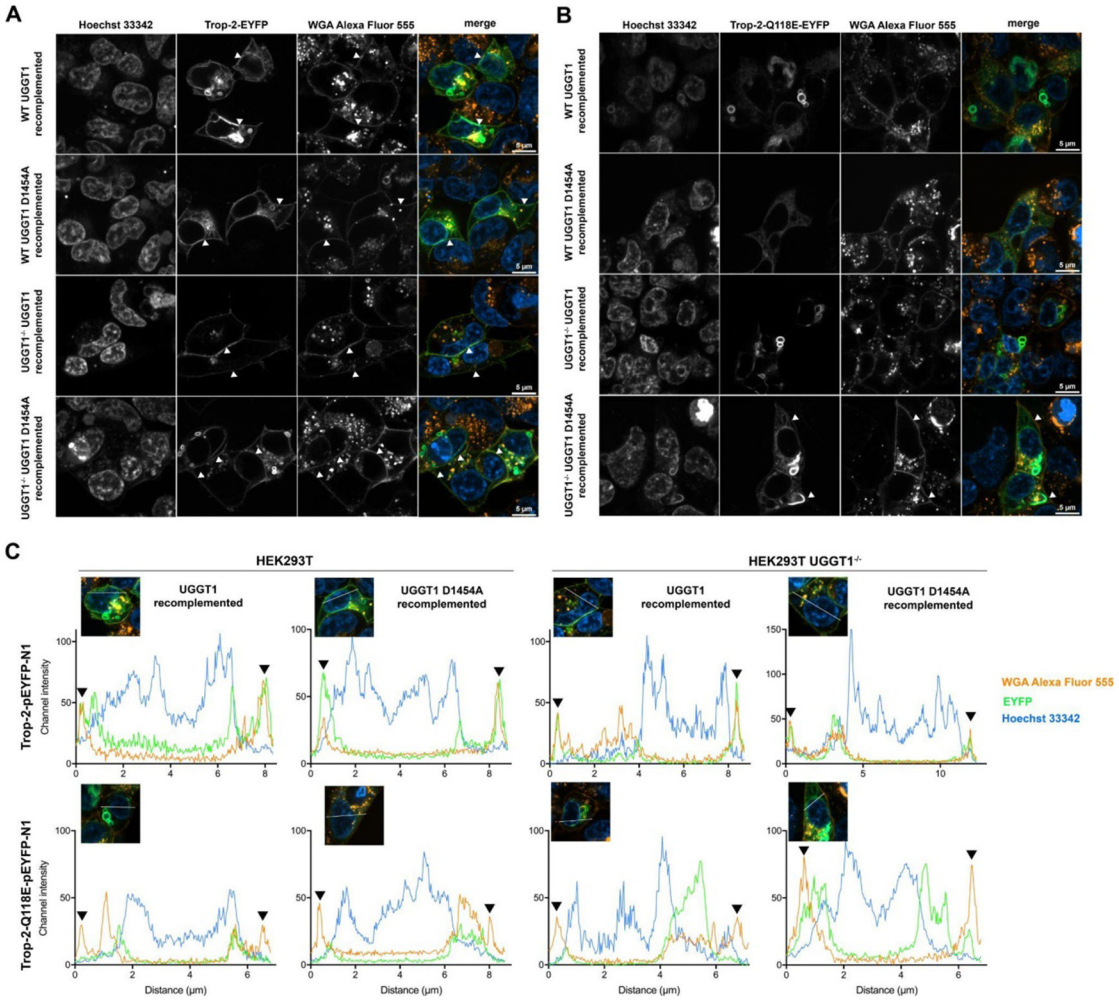

Figure 3. The Trop-2-Q118E-EYFP lack of secretion phenotype is restored in HEK293T *UGGT1*$^{-/-}$ cells complemented with the *UGGT1* gene.

(A): UGGT1 and UGGT1 D1454A complementation does not interfere with the localisation of the WT Trop-2-EYFP glycoprotein (green): the protein traverses the secretory pathway and reaches the plasma membrane (white arrowheads);**(B):** In complemented WT cells, the Trop-2-Q118E-EYFP mutant glycoprotein (green) is absent from the plasma membrane and is retained in the secretory pathway (top first and second rows). In the complemented *UGGT1*$^{-/-}$ cells, we observe restoration of the original lack of secretion phenotype observed for Trop-2-Q118E-EYFP in WT cells: the Trop-2-Q118E-EYFP mutant glycoprotein does not reach the plasma membrane (third row). Consistently with these observations, we still observe the rescue of secretion of the mutant glycoprotein in *UGGT1*$^{-/-}$ cells complemented with the inactive UGGT1 D1454A mutant (bottom row, white arrowheads). **(C):** Multichannel intensity plots of the Trop-2-EYFP transfected complemented cell lines confirm our visual observations (black arrowheads).

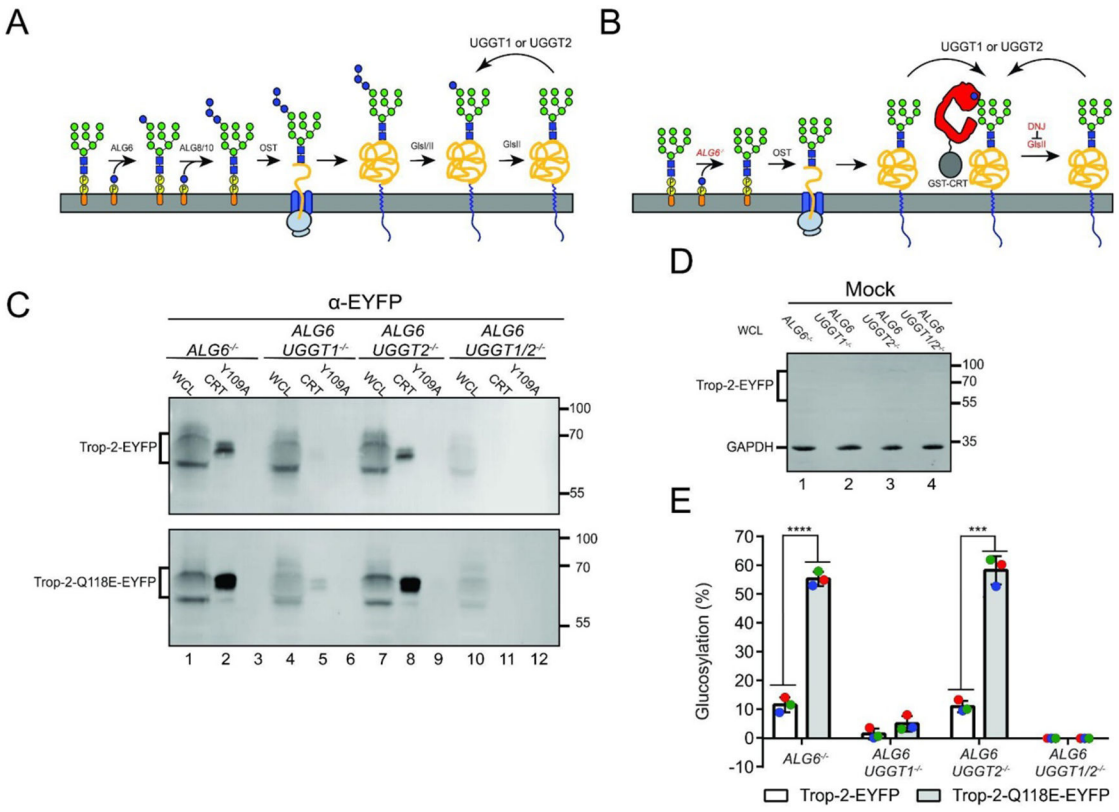

Figure 4: The *in cellula* glucosylation by UGGT1 of Trop-2-EYFP (WT and Q118E mutant).
(A): The synthesis and modification of *N*-linked glycans starting from the dolichol-P-P-$Man_9GlcNAc_2$ stage within the ER lumen. ALG6 appends the first glucose onto the immature glycan using dolichol-P-glucose as the source. The mono-glucosylated glycan is then built into a tri-glucosylated carbohydrate by ALG8/10 prior to covalent linking to the nascent peptide chains. The glycan is trimmed to a mono-glucosylated state by glucosidases I and II, whereupon it can bind ER lectin chaperones. Removal of the remaining glucose by glucosidase II dissociates the glycoprotein from the lectin chaperones, whereby three options are possible: continuation of trafficking, degradation, or reglucosylation by the UGGTs. Orange ovals represent dolichol anchors, yellow circles phosphates, blue squares GlcNAc, green circles mannose, and blue circles glucose. **(B):** Alteration of glycan synthesis pathway for glucosylation studies. Deletion of *ALG6* results in a $Man_9GlcNAc_2$ glycan being transferred to nascent chains by the OST as the initial glucose can no longer be added. Interaction with ER lectin chaperones is thereby facilitated solely through glucosylation by the UGGTs. Further enrichment is achieved through treatment with DNJ, preventing the removal of the inner glucose. **(C):** The designated cell lines were transfected with either the WT Trop-2-EYFP or Q118E mutant and lysed. The lysate was split between a whole cell lysate (WCL) sample (20%) and a GST-CRT (35%) and GST-CRT-Y109A pulldown (35%) and resolved by 9% SDS-PAGE before transferring to a PVDF membrane. Imaged is an αEYFP immunoblot. Data represent three independent biological replicates. **(D):** Mock transfection to measure background binding of αEYFP antibody against whole cell lysate from each cell line. The membrane was also probed against GAPDH as a loading control. **(E):** Quantification of blots from **(C)**. Percent glucosylation was calculated by subtracting

the amount of protein pulled down in the Y109A lane from the CRT for each cell line. The resulting value was divided by the normalised quantified protein within the whole cell lysate and multiplied by 100. Error bars represent the standard deviation. **** represents $P \leq 0.0001$ and *** represents $P \leq 0.001$.

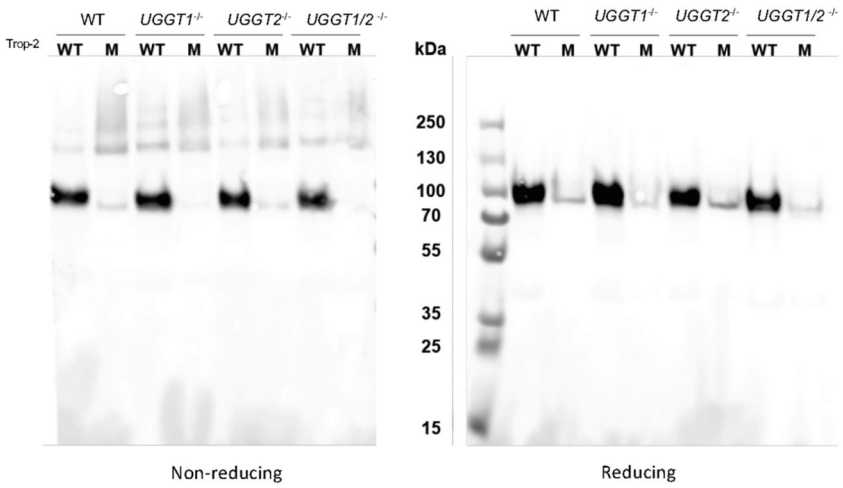

Figure 5. The Q118E mutation generates inter-molecularly SS-bonded misfolded Trop-2-Q118E-pEYFP-N1 multimers.

Anti-EYFP Western blot of membrane fractions extracted with the CelLytic™ MEM Protein Extraction Kit from HEK293T cells transiently transfected with the Trop-2-pEYFP-N1 ("WT") and Trop-2-Q118E-pEYFP-N1 plasmids ("M"). Samples were run in the absence or presence of reducing agent (50 mM DTT).

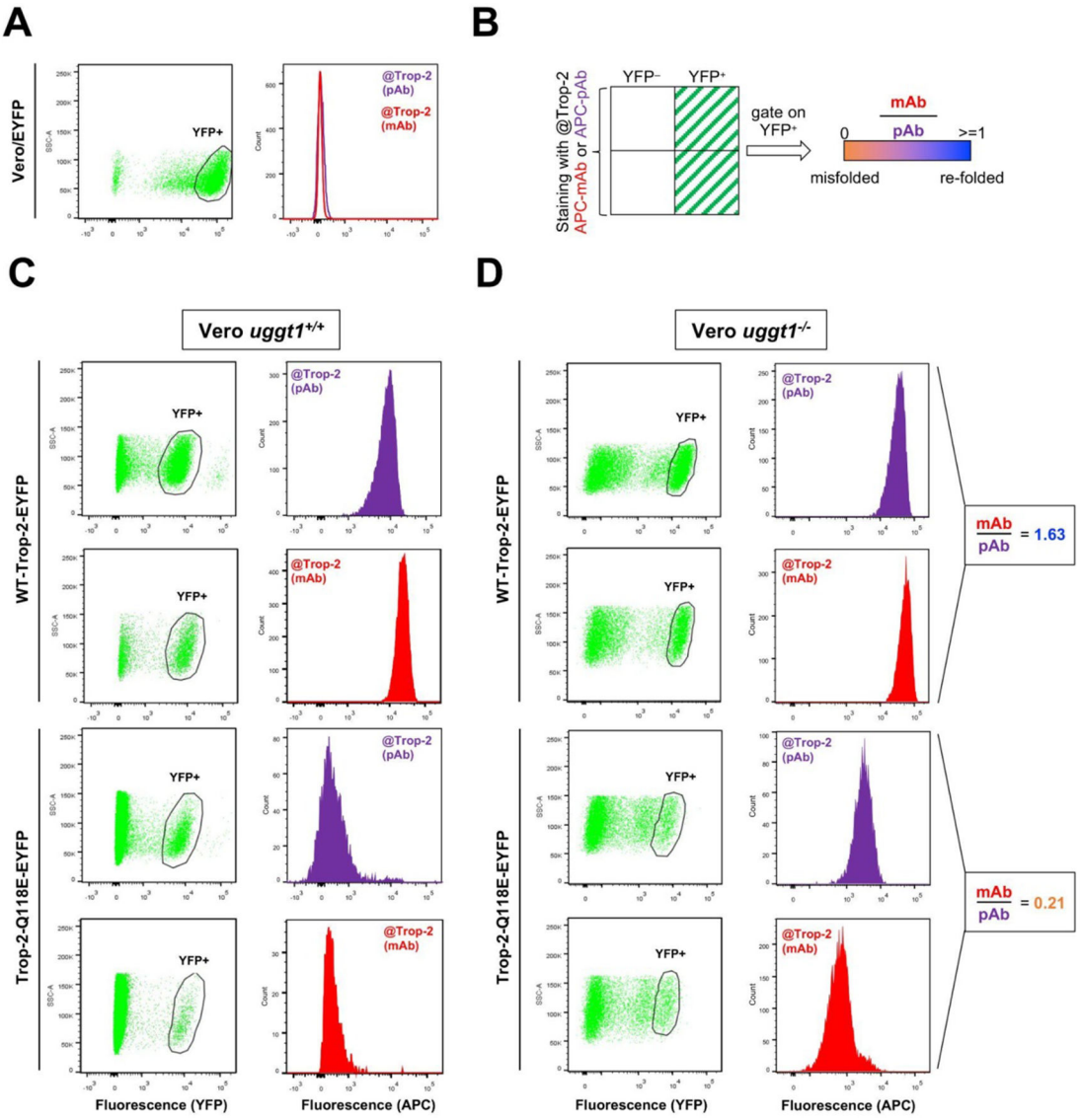

Figure 6. Assessment of the secretion-rescued Trop-2 folding.

(A): Vero E6 cells transfected with EYFP and stained with either monoclonal (mAb) or polyclonal (pAb) antibodies against Trop-2. **(B):** Summary of the gating and signal acquisition strategy. **(C,D):** Left panels: dot plots of the experiments showing the YFP+ cells that were gated out for the subsequent analysis. Right panels: histogram plots showing the expression levels of membranous Trop-2 as measured by staining with an anti Trop-2 pAb (purple) or mAb (red). Ratios between mAb and pAb Mean Fluorescence Intensities are shown for each experimental group. Left, analysis on *UGGT1*$^{+/+}$ cells.Right, analysis on *UGGT1*$^{-/-}$ cells.

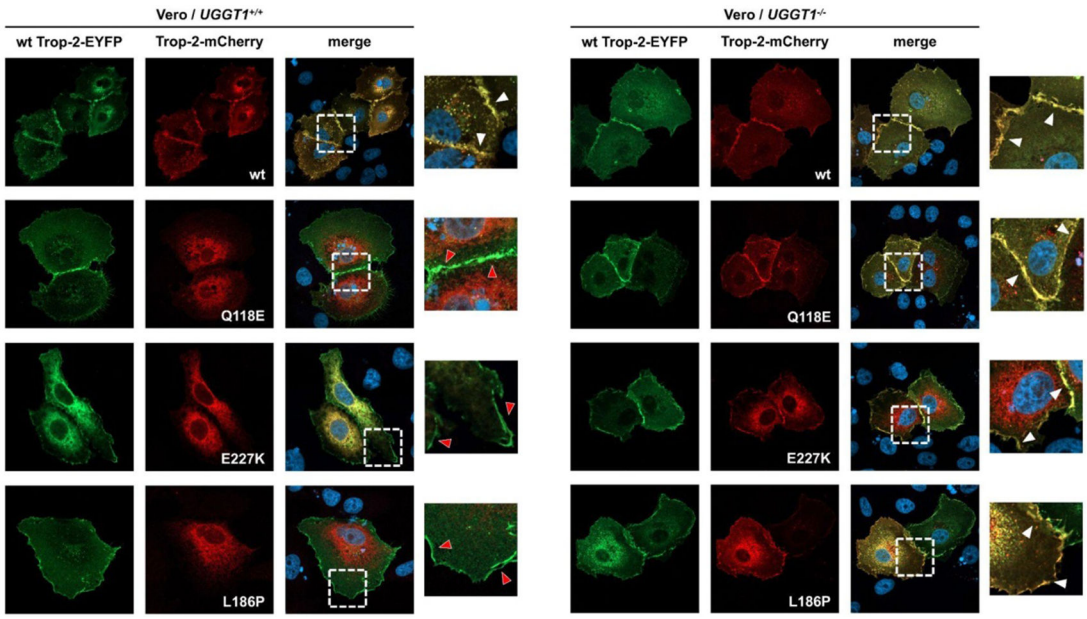

Figure 7. Confocal microscopy of WT Trop-2 and Trop-2 Q118E, E227K and L186P mutants in Vero E6 cells.

Cellular localisation was assessed in *UGGT1*$^{+/+}$ (left) and *UGGT1*$^{-/-}$ (right) Vero E6 cells by confocal microscopy. Cells were imaged upon co-transfection of WT Trop-2-EYFP (to track baseline localisation of the WT molecule) and WT/mutant Trop-2-mCherry fusion proteins (to track mutants with WT Trop-2). Mutant Trop-2 molecules were retained in intracellular compartments of the *UGGT1*$^{+/+}$ cells (left), but reached the plasma membrane in *UGGT1*$^{-/-}$ cells. WT Trop-2-EYFP and WT Trop-2-mCherry co-localise at the plasma membrane independently on the presence or absence of UGGT1, as expected. White arrowheads: areas of membrane co-localisation. Red arrowheads: absence of co-localisation between WT Trop-2-EYFP and the mCherry Trop-2 mutant fusion proteins.